Int. J. Human–Computer Studies 188 (2024) 103273

Contents lists available at ScienceDirect

International Journal of Human - Computer Studies

journal homepage: www.elsevier.com/locate/ijhcs

Editorial

EEBA: Efficient and ergonomic Big-Arm for distant object manipulation in VR

Jian Wu [a], Lili Wang [a,b,*], Sio Kei Im [c], Chan Tong Lam [c]

[a] State key laboratory of virtual reality technology and systems, Beihang University, 100191, Beijing, China
[b] Peng Cheng Laboratory, Shenzhen, 518052, Guangzhou, China
[c] Macao Polytechnic University, Macao, 999078, Macao Special Administrative Region of China

ARTICLE INFO

Keywords:
Virtual reality
Interaction
Object manipulation
Efficient
Ergonomic

ABSTRACT

Object manipulation is the most common form of interaction in virtual reality. We introduced an efficient and ergonomic Big-Arm method to improve the efficiency and comfort of manipulating distant objects in virtual reality. We prolong the upper arm and forearm lengths according to the maximum distance of the manipulation space and construct the linear mapping between the real and virtual elbow angle, which makes manipulation easier to control and more efficient. We propose an optimized elbow angle mapping to further improve the efficiency and comfort of distant object manipulation. Two user studies were designed and conducted to evaluate the performance of our optimized Big-Arm method. The results show that our method achieves significant improvement in efficiency, ergonomic performance, and task load reduction for manipulating the distant object (distance ≥6 m) compared to the state-of-the-art methods. At the same time, our method exhibits superior usability.

1. Introduction

Virtual object manipulation is one of the fundamental interactions in virtual reality (VR) and has been studied for a long time. Researchers have devoted themselves to finding better ways to manipulate (translate, rotate, and scale) virtual objects (Frees and Kessler, 2005; Jacoby et al., 1994). Distant virtual object manipulation has more challenges because the user cannot reach the object directly (Poupyrev et al., 1996). Therefore users have to use other tools to catch the objects, such as the casting-ray-based method (Bowman and Hodges, 1997), in which objects are bound on the tip of the cast ray. By pointing the ray in a particular direction and pressing related buttons to change the ray length, users can translate the objects to their desired positions. The Go-Go type methods, like Go-Go (Poupyrev et al., 1996), 3D cursor (Li et al., 2015, 2018) were proposed, which manipulate the distant virtual objects more directly. However, they still have some disadvantages.

As shown in Table 1, casting-ray-based techniques prove less efficient when it comes to relocating virtual objects over substantial depths, mainly due to the considerable time required for adjusting the ray length. On the other hand, in methods resembling Go-Go, users frequently find themselves extending their arms for an extended period, especially when objects are positioned near the boundaries of reachable space. Such prolonged motion can lead to user fatigue. Hence, the need for a novel method to address these challenges becomes evident.

We considered three design requirements to improve object manipulation's efficiency, accuracy, and comfort. First, to improve the efficiency of the interaction, the user should be able to manipulate the object with just one smooth action. Previous Go-Go-like methods manipulate objects with a straight rod, which leads to a two-step action: pointing in the direction and then adjusting the length to catch. The two-step action generally takes more time than a single action. So, we intend to design a method in which users can catch the objects with only one smooth action. Second, the visual feedback of the method should provide a comprehensive cue for the users to better mentally map their real arms to the virtual arms movement, reducing the controlling difficulty and improving the manipulation efficiency (Rosenbaum, 2009; Franklin and Wolpert, 2011). Generally, to control movement, the nervous system must integrate multimodal sensory information. However, in a VR system, users can only see their virtual "arms." If the virtual "arms" cannot provide comprehensive visual feedback, users may not successfully control motor movement, which is crucial to interacting with the objects. Third, the user's movement should be natural and ergonomic, especially for manipulating the object far away, offering a low task load and considerable usability. Since there are certain arm-moving areas that humans can feel comfort when applying daily activities (Morrey et al., 1981, 2000; Montano Murillo et al., 2017).

Following the three design requirements, we introduce an efficient and ergonomic Big-Arm (EEBA) metaphor for manipulating distant objects in VR. Using the tracked HTC Vive head-mounted display, the

* Corresponding author at: State key laboratory of virtual reality technology and systems, Beihang University, 100191, Beijing, China.
E-mail addresses: lanayawj@buaa.edu.cn (J. Wu), wanglily@buaa.edu.cn (L. Wang), marcusim@mpu.edu.mo (S.K. Im), ctlam@mpu.edu.mo (C.T. Lam).

https://doi.org/10.1016/j.ijhcs.2024.103273
Received 12 June 2023; Received in revised form 4 April 2024; Accepted 8 April 2024
Available online 25 April 2024

Table 1
Comparison for indirect and direct manipulation variants.

Method type	Representatives	Pros	Cons
casting-ray-based	Bowman and Hodges (1997)	fast selection	difficult ray length control, long segmented trajectory
Go-Go type	Poupyrev et al. (1996), Li et al. (2018)	intuitive length control	two-step manipulation, tired at a large distance, movement mapping is hard to grasp

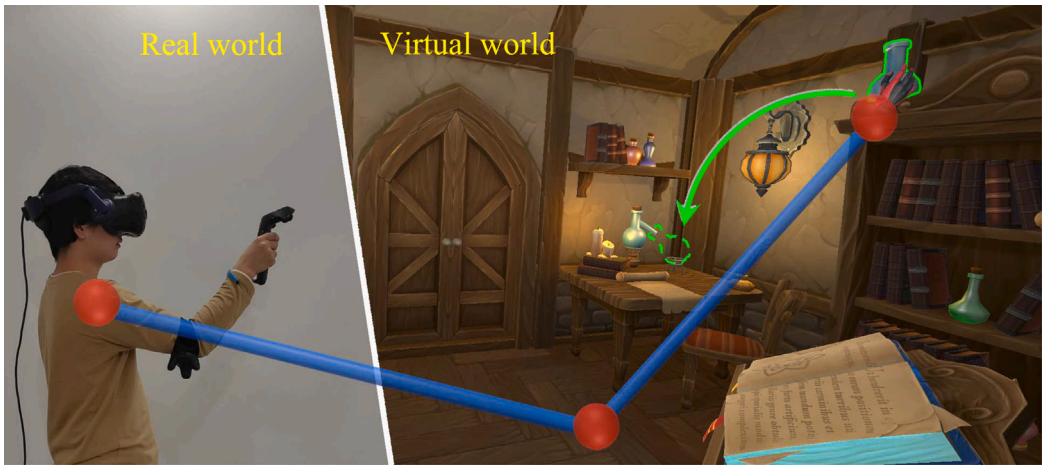

Fig. 1. EEBA metaphor. Using one additional tracker with the HMD and controller, the user's arm is tracked and mapped into the virtual EEBA metaphor (represented with the blue sticks and red spheres). With the EEBA metaphor, the user can grasp the faraway bottle on the bookshelf and translate it to the target position (marked with green dotted outlines) efficiently and ergonomically.

controllers, and one HTC Vive tracker bound on the elbow joint (Fig. 1), we capture the user's arm motion (including shoulder, elbow, and wrist motions). Inspired by the Giant walking (Abtahi et al., 2019), which scales the user into a virtual giant for fast navigation, we then prolong the upper arm and forearm lengths according to the maximum distance of the manipulation space and construct the linear mapping between the real and virtual elbow angle. Therefore the user can reach the whole manipulation space and manipulate the virtual arm just like in life due to the same mechanical linkage structure. The virtual arm length remains constant during manipulation, so the user can easily predict the object's motion according to the bending of the virtual arm. In order to further improve the efficiency and comfort of distant object manipulation, we optimize the real and virtual elbow angle mapping. We propose an empirical function model between the real elbow angle and the object's final position adjusting time and then conduct a pilot user study to fit it. With the fitted model, we propose an optimized ergonomic elbow angle mapping function, which enables users to manipulate distant objects with a more comfortable arm position, reducing manipulation time. We conducted two controlled user studies to evaluate the performance of our method. The results show that our method significantly improves efficiency and ergonomic performance for manipulating the distant object (distance≥6 m) compared to the state-of-the-art methods. Our method reduces the task load significantly for manipulating the object at all tested distances and shows comparable usability performance compared to the state-of-the-art methods. Fig. 1 shows how our EEBA method works. The user is controlling the EEBA metaphor to grasp the bottle on the top of the bookshelf and then transport it to the target location (marked with green dotted outlines) in the virtual environment.

The contributions of this paper are summarized as follows:

- We introduce a Big-Arm interaction metaphor, which provides intuitive visual feedback, enhances users' spatial awareness and ability to control the virtual hand efficiently and improves manipulation efficiency.
- We propose an optimized virtual–real elbow angle mapping function, which improves the manipulation comfort and efficiency.

In the following, we first introduced the prior work on distant object manipulation in Section 2. Then, we propose our EEBA method in Section 3. Section 4 designs a pilot user study to fit our method model. After that, we conducted two user studies to evaluate the performance of our method in Sections 5 and 6. Finally, we conclude and discuss the limitations and future work in Section 7.

2. Related work

Distant object manipulation has been studied for decades, and many techniques have emerged and demonstrated their respective advantages. Here, we divide the techniques into two categories: indirect manipulation and direct manipulation, and then briefly discuss related prior work. For a more comprehensive illustration, we recommended readers to the survey paper (Mendes et al., 2019).

2.1. Indirect manipulation

The indirect manipulation method has the feature that the target object's motion is not directly mapped to the user's hand movement. Usually, they are connected by some tools, like rays, mirrors, replicas, etc. One of the techniques is the Worlds in Miniature (WIM), which provides a hand-held miniature representation of the virtual world. The users can manipulate the inside tiny objects in their hands (Stoakley et al., 1995). Pierce et al. introduced Sticky Finger, allowing distant object selection using the thumb and index finger (Pierce et al., 1997), and then allowing the manipulation in space. Another similar work is the Voodoo Dolls (Pierce et al., 1999), which allows users to manipulate remote objects with their copied dolls in their hands. Recent work scaled down the whole virtual world to enable manipulation with distant and occluded objects (Yu et al., 2019). Another Poros method introduces a space proxy method (Pohl et al., 2021). By constructing several marked spaces, the user can manipulate the distant objects in

the space proxies nearby. Although these methods solve the problem of distance, they break the spatial relation between users and virtual objects. For WIM and Voodoo Dolls, users have to switch their views a lot when adjusting the positions of the objects in the virtual environment.

Another approach for moving distant virtual objects is the sliding-based method. The method moves an object along a chosen plane/surface by pressing on the trackpad (Sun et al., 2016). Then, the extended sliding-based method introduces a fine adjustment phase to map the 3d movement of the hand (Sun and Stuerzlinger, 2019). However, the manipulation process becomes complicated since these two methods need a predefined plane or a chosen surface in the virtual environment.

Some approaches use additional tools to contact the target object in order to maintain the positional relationship between it and the user. The most commonly used tool is a ray. By emitting a ray to the target object, the user can easily select the target and then manipulate it (Mine, 1995; Bowman and Hodges, 1997; Liu et al., 2022). Based on ray casting, the HOMER method is proposed to facilitate easier control of the ray length by attaching the hand to the target object on the ray and then linearly mapping the hand motion to the object motion (Bowman et al., 1999). However, the farthest distance the user can reach is limited by the length of his upper limbs, making it difficult to move virtual objects to a distant target location in a single operation. A velocity-based scaling strategy is applied to the ray length to increase the manipulation efficiency (Wilkes and Bowman, 2008). Yu et al. proposed a gesture-based remote object manipulation technique, Force Push, which uses different gestures to control the object movement (Yu and Bowman, 2018). However, its controllability and accuracy were considered inferior to direct control. Yu et al. proposed the alpha cursor method to select fully occluded target objects by cutting away virtual geometries inside a clipping sphere (Yu et al., 2020). Recently, Li et al. proposed vMirror, which enables distant or occluded VR object manipulation with an interactive widget leveraging the reflection of mirrors (Li et al., 2021). By placing the virtual mirrors in the scene, users can select target objects, even occluded, by pointing rays at the reflected images in the mirrors. These ray-based methods keep the spatial relation between target objects and the users unchanged. They are good at target object selection missions. However, when it comes to object manipulation, the users have to control the movement of the objects by indirectly changing the direction, length of the ray, orientation, and location of the mirror or using the buttons of the controller, which makes the manipulation inconvenient and inefficient.

The indirect manipulation method does not directly manipulate the target object by hand motion, so there is a specific learning cost. Although they can select the objects easily, some of the methods may also suffer from inefficiency when moving virtual objects.

2.2. Direct manipulation

The direct manipulation methods map the target object's motion to the movement of the user's hand. For distant objects, the most direct idea of direct manipulation is to send the user to the nearby region of the virtual object with the help of walking or teleportation techniques (Bolte et al., 2011; Bozgeyikli et al., 2016). Then the user can manipulate the object directly through hand movements. However, teleportation needs additional user viewpoint translation, which leads to an extra task load for users, and it is also inefficient. To address the problem, gaze-supported object manipulation methods have been widely studied (Chatterjee et al., 2015; Velloso et al., 2015; Voelker et al., 2020; Yu et al., 2021). For example, Yu et al. proposed gaze-supported techniques for distant object manipulation, allowing users to select objects with their eyes and then manipulate them by hand (Yu et al., 2021). The combination of gaze and hand inputs helps avoid unnecessary viewpoint teleportation and can be helpful for large environments with distant target objects (Turner et al., 2011, 2013). However, it also suffers disadvantages, such as that users have to focus their eyes on the target objects, which may increase eye strain during the manipulation tasks or cause loss of virtual scene context. Furthermore, the joint interaction of the eye and hand limits the manipulation accuracy and efficiency.

Another direct manipulation method of distant objects is by hand in mid-air. It focuses on manipulating distant objects in comfortable hand poses. Feuchtner et al. proposed the Ownershift technique, which allows users to interact with overhead target objects with their hands placed down at a comfortable position (Feuchtner and Müller, 2018). The Erg-O technique remaps the nearby virtual space and amplifies movement to help users reach the boundary area at a natural reaching area (Montano Murillo et al., 2017). These two methods shift the user's hand position to some comfortable location and reduce the user's task load. However, since the hand comfort space is similar in size to the interactive virtual space in mapping, they are not good at long-range object translation interaction.

To directly manipulate distant target objects, many approaches amplify the virtual arm's length to reach distant objects. A typical method is the Go-Go technique, which grows the vector along the hand direction to reach and manipulate distant objects (Poupyrev et al., 1996). Then, Li et al. introduced the Linear Offset method, a Go-Go variation that optimized the mapping and outperformed the former (Li et al., 2015, 2018). Wentzel et al. proposed a configurable Hermite curve function to help maintain body ownership when amplifying the motion of the hands (Wentzel et al., 2020). Further, Feuchtner et al. investigated how appearance, realism, and connectivity of the stretched long arm contribute to the perception of ownership in AR applications (Feuchtner and Müller, 2017), and Dewez et al. studied the impact of using a dual body representation during both close and distant manipulations (Dewez et al., 2022). These methods work on amplifying the virtual hand positions, focusing mainly on new mapping functions to the original Go-Go metaphor. The limitation of these methods is that they magnify the length along a straight line to achieve the goal of changing position, which ignores the fact that the motion of the human arm is a linkage motion that rotates around the elbow joint and is therefore not intuitive for the control of the hand motion.

Our EEBA method is also a direct manipulation method for distant objects. The structure of our EEBA metaphor is a linkage, which is the same as the real human arm. This similar structure brings several advantages. First, the same structure means the same control method. Users can quickly grab the key points of controlling the metaphor. Second, the visual feedback of the metaphor is also in line with the real arm. When users extend their real arms, the virtual arms also extend, and vice versa. This ensures instant and comprehensive visual kinematic feedback for the users to construct a reflex-based controlled movement (Schmidt and Wrisberg, 2008). We intend to propose an efficiency-improved and ergonomically friendly manipulation method.

3. Method

This section describes the details of our EEBA method based on the three design requirements above. First, we propose the basic Big-Arm prototype and then introduce the optimized ergonomic elbow mapping function to improve its comfort and efficiency.

3.1. Basic Big-Arm

Based on the first two design requirements, to offer a comprehensive visual cue to the user, we define the Big-Arm metaphor as a prolonged virtual fixed-length arm divided into an upper arm and a forearm like a real arm. As shown in Fig. 2, (a), we abstract the human arm as a link structure with a six-tuple $(s,\ e,\ w,\ u,\ f,\ \beta)$, where s, e, w, represent the joint of the shoulder, elbow, and wrist, u, f represent the linked upper arm and forearm, β represents the real elbow angle. Analogous to a real arm, our Big-Arm can also be represented with a six-tuple $(s',\ e',\ w',\ u',\ f',\ \beta')$, representing the virtual shoulder, elbow, wrist, upper arm,

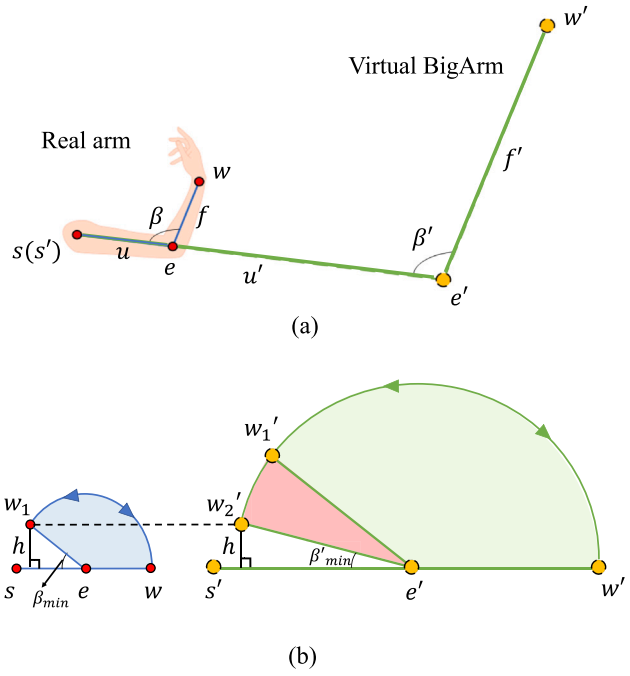

Fig. 2. (a) The basic structure of the virtual BigArm. $s(s'), e(e'), w(w'), u(u'), f(f'), \beta(\beta')$ represent the shoulder, elbow, wrist, upper arm, forearm, and elbow angle of the physical (virtual) arm. The shoulder locations are aligned. (b) The virtual BigArm metaphor can only cover the green range if we apply a 1:1 elbow angles mapping. We want to reduce the minimum value of the virtual elbow angle β'_{min} to reach the residual range marked in red.

forearm, and elbow angle, as the same meaning as the corresponding parameters of the real arm. When the user wants to stretch the virtual arm, he/she only needs to stretch his arm in the real world, and vice versa. The fixed-length limbs provide visual feedback for virtual hand movement. Just as in reality, by observing the arm movements, the user can perceive where the hand will be. Furthermore, the kinematic form of the virtual arm is similar to that of the real arm, both of which are joint-rod structures hinged at the elbow. These designs help the user understand and control the virtual arm's movement and facilitate the user's planning of the virtual arm's movement path.

In order to obtain the parameters of the real arm, the HTC Vive Pro 2 HMD, one handheld controller, and one HTC Vive tracker are used (Fig. 1). s is calculated from the user's head position and orientation tracked by HMD, the preset user's neck length, and shoulder width. e is tracked with the HTC Vive tracker bound on the elbow of the user, and w is captured with the handheld controller. u, f, and β can be calculated with s, e, and w.

We construct the virtual arm (s', e', w', u', f', β') based on the real arm (s, e, w, u, f, β). The shoulder s' is fixed at the same position as the real shoulder s. The direction of the real and virtual upper arms are the same. Then we need to determine the virtual upper arm length u', the virtual forearm length f', and the virtual elbow angle β'. Finally, e' and w' can be calculated according to them.s

To calculate u' and f', we set the total length of the virtual arm the same as the maximum distance $D_m = u' + f'$ associated with a specific task. For example, in Fig. 1, D_m is set as the maximum length of the virtual room. Then, divide the virtual arm proportionally to the user's forearm and upper arm ($u'/u = f'/f$).

To calculate β', the most intuitive mapping method is the 1:1 mapping ($\beta' = \beta$). As shown in Fig. 2, (b), When the real arm is bent to the minimum elbow angle (β_{min}), the virtual Big-Arm can only reach the boundary of the green area (w'_1) with the 1:1 mapping, resulting in the inability to manipulate objects in the red region close to the user, which is constructed by setting the same distance h from the real wrist w_1 to the real upper arm. To make the virtual Big-Arm cover the entire region (red and green, $\beta' \in [\beta'_{min}, 180°]$), we need to construct a linear mapping between the virtual and the real elbow angle. We align the maximum and minimum values of the virtual and real arm elbow angles and then map the intermediate range of angles by linear interpolation. Following the above designs, we can calculate u', f', β' as follows:

$$\begin{cases} k = D_m/(u+f) \\ u' = ku, f' = kf \\ \beta'_{min} = arcsin\frac{f\,sin\beta_{min}}{f'} = arcsin\frac{sin\beta_{min}}{k} \\ \beta' = \frac{\beta-\beta_{min}}{\pi-\beta_{min}}(\pi-\beta'_{min}) + \beta'_{min} \end{cases} \tag{1}$$

Here, k represents the prolonged ratio between the real and virtual arms. Row 3 shows how to calculate the minimum virtual elbow angle, which is inferred from the equation ($h = f\sin\beta_{min} = f'\sin\beta'_{min}$). Row 4 gives the linear mapping function. When $\beta = \pi$, $\beta' = \pi$. When $\beta = \beta_{min}$, $\beta' = \beta'_{min}$.

3.2. Elbow angle mapping optimization

We optimize the elbow angle mapping according to the third design requirement. First, we reset an ergonomic elbow angle range and then propose an optimized elbow angle mapping function according to the performance of the basic Big-Arm method.

3.2.1. Ergonomic elbow angle range

An ergonomic-friendly design means the user can access any accessible virtual location with a relatively comfortable real-world arm pose (Montano Murillo et al., 2017). According to previous studies, people can accomplish most of the activities of daily living with 100 ° of elbow flexion (from 50° to 150°) (Morrey et al., 2000, 1981). Beyond this range, the user's arm is prone to discomfort or fatigue.

Based on the above findings, we reset the real elbow angle mapping range to $\beta \in [50°, 150°]$. When the user's elbow angle reaches minimum value $\beta_{min} = 50°$, the virtual elbow angle also reaches the minimum β'_{min}, calculated with Eq. (1). When the user's elbow angle reaches maximum value $\beta_{max} = 150°$, the virtual elbow reaches the maximum $\beta'_{max} = \beta_{max}$ to keep the user's perception of boundaries consistent.

From Fig. 2, according to the Pythagorean theorem, the reach distance d of the BigArm can be represented as:

$$\begin{aligned} d &= |s' - w'| \\ &= \sqrt{[u' + f'cos(\pi-\beta')]^2 + [f'sin(\pi-\beta')]^2} \end{aligned} \tag{2}$$

Replace d with D_m, $\beta' = 150°$ and $k = \frac{u'}{u} = \frac{f'}{f}$, the prolonged ratio k is updated as

$$k = \frac{D_m}{\sqrt{u^2 + f^2 + \sqrt{3}\cdot u\cdot f}} \tag{3}$$

3.2.2. Optimized elbow angle mapping function

We performed several informal tests on the basic Big-Arm prototype by translating virtual objects to some target locations with different user–target distances d_{ut}. During the translation, we recorded the time cost and trajectories of the objects. Typical time cost and trajectory data for translating three objects located at different distances (d_{ut} = 2 m, 4 m, 6 m) are shown in different colors yellow, blue, and green in Fig. 3.

According to the results, we have two findings:

- The translating process of the object can be divided into two stages. When the object is far from the target location, the moving speed is fast since participants can ignore the accuracy requirement. When the object is near the target location, they have to slow down to place the object accurately (Graham and MacKenzie, 1996). In the first stage, the object rapidly approaches the

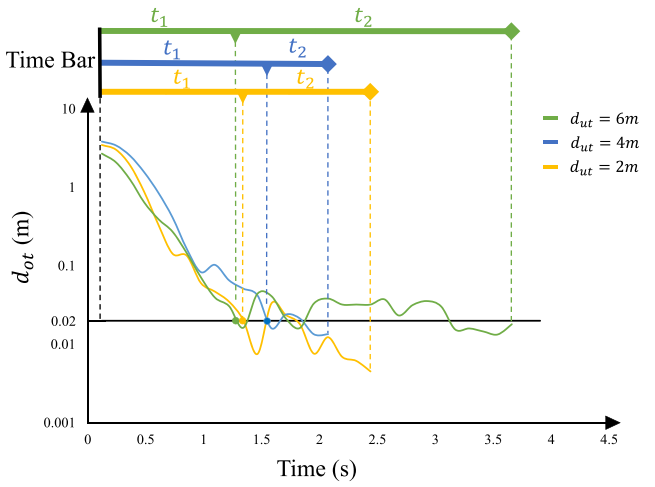

Fig. 3. The typical time costs and trajectory data of three objects with different d_{ut}: 2 m, 4 m, and 6 m. d_{ot} represents the distance between the object and the target location. The total length of the virtual arm is set as $D_m = 6.5$ m in the tests. The Time Bar shows the time costs for the coarse approaching stage (t_1) and the fine-tuning stage (t_2).

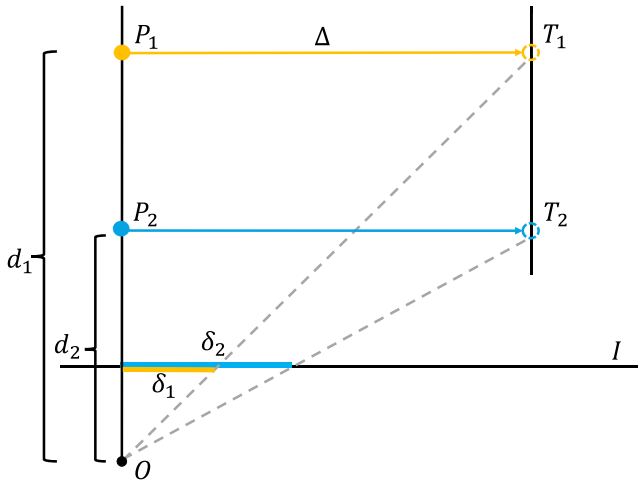

Fig. 4. The projected translating path lengths δ_1 and δ_2 on the image plane I of the virtual objects P_1 and P_2 for the same path length Δ. The distances for P_1 and P_2 from the user position O are d_1 and d_2.

target position with a time cost of t_1. The distance between the object and the target d_{ot} rapidly decreases. The second stage of the fine-tuning process starts when the object is moved for the first time to the area near the target (we set $d_{ot} \leq 0.02$ m in our tests). In this process, the user decreases the hand-moving speed to make the manipulated object coincide with the target. Due to the inertia of the hand movement, the trajectory of the fine-tuning process oscillates until the user presses a button to confirm the end of the translation. The time cost of this stage is noted as t_2.

- Compared to t_1, when the distance from the target location to the user (d_{ut}) increases, t_2 changes drastically, first decreasing and then increasing. This is because it is easier for the user to manipulate when the user's elbow angle is around 90° ($d_{ut} = 4$ m), and the greater the deviation ($d_{ut} = 2\,\text{m}, 6$ m), the more difficult it is to manipulate (Morrey et al., 1981, 2000). When users stretch or bend their arms significantly to manipulate the virtual objects, the increasing t_2 reduces the manipulation efficiency.

Based on the above findings, reducing t_2 time in the fine-tuning stage is necessary to improve the manipulation efficiency when d_{ut} is small or large. The main idea of our elbow angle mapping optimization is to construct a new mapping between β' and β to reduce the fine-tuning process time t_2. The construction process consists of two steps.

The first step is to model the relationship between t_2 and β, with the pilot user study results when applying the basic Big-Arm method. According to the second finding above, t_2 first decreases and then increases when β increases. We approximate this underlying trend using a quadratic function (Eq. (4), left half). Another factor that may influence t_2 is the distance from the target to the user d_{ut}. In Fig. 3, when d_{ut} increases from 4 m to 6 m, t_2 increases more than when d_{ut} decreases to 2 m. The reason is shown in Fig. 4. O is the eye position of the user, P_1, P_2 are two virtual objects with different distances ($d_1 > d_2$) from the user. T_1 and T_2 are the corresponding target locations for P_1 and P_2. I is the image plane. Although the translating length in the 3D space (Δ) from P_1 to T_1 and P_2 to T_2 are the same, the projected path lengths are different $\delta_1 < \delta_2$.

The user relies mainly on visual feedback (object–target projection image) for object manipulation adjustments. In order for the user to detect the difference between the object and the target position, a sufficiently large image variation is required. In the second stage, the object enters the area near the target. The further away the target is, the smaller its projection change is and the more difficult it is for the user to discern the change, hence the longer the manipulation time t_2. For simplicity, we assume that t_2 is linearly proportional to d.

So far, we model the relation between t_2 and β as:

$$t_2 = (e_1\beta^2 + e_2\beta + e_3) \cdot \sqrt{e_4 - e_5 cos(e_6\beta + e_7)} \tag{4}$$

The left half is the quadratic function, and the right half is a weighted d, which is inferred from Eqs. (1) and (2). e_1 to e_7 are undetermined coefficients, and we will fit them with a pilot user study in Section 4.

The second step is to construct the new mapping function between β' and β. Our Big-Arm metaphor enables the controlling of the virtual arm by amplifying the real elbow angle β to the virtual elbow angle β'. In the fine-tuning stage, the amplifying ratio $\frac{d\beta'}{d\beta}$ can influence the easiness of controlling the Big-Arm. The smaller the ratio, the easier it is to control the Big-Arm, resulting in decreasing t_2. So, we proposed our new mapping function as an integral function of $1/t_2$:

$$\beta' = a \int \frac{1}{t_2} d\beta + b \cdot \beta \tag{5}$$

Where a, b are coefficients related to the virtual minimum elbow angle β'_{min}. a and b can be calculated with the following equation group:

$$\begin{cases} \beta'_{max} = a \int_{\beta_{min}}^{\beta_{max}} \frac{1}{t_2} d\beta + b\beta_{max} \\ \beta'_{min} = a \int_{\beta_{min}}^{\beta_{max}} \frac{1}{t_2} d\beta + b\beta_{min} \end{cases} \tag{6}$$

Since the minimum and maximum real and virtual elbow angles are known, we can solve the equation group easily and get the coefficients a and b.

4. Pilot user study: Fitting model

4.1. Overview and hypotheses

The pilot user study has two stages. In the first stage, we tested the manipulation performance of the basic Big-Arm method to fit the pending coefficients illustrated in Eq. (4). In the second stage, we constructed our EEBA method using the fitted parameters and tested its performance. The performance data collected from the two methods were compared to validate the following hypotheses:

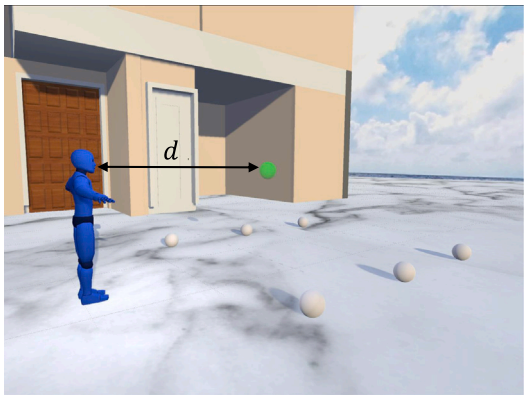

Fig. 5. The scene layout in the pilot user study. Participants (the blue avatar) were asked to translate the six white spheres on the ground to the target location, rendered as a transparent green sphere. We set 8 target locations for each participant, and the distances are $d \in \{0.5\text{ m}, 1\text{ m}, 2\text{ m}, 3\text{ m}, 4\text{ m}, 5\text{ m}, 5.5\text{ m}, 6\text{ m}\}$.

H0-a. EEBA method is able to reduce the coarse approaching time t_1 compared with the basic Big-Arm method.

H0-b. EEBA method is able to reduce the fine-tuning adjusting time t_2 when the target distance is near the max manipulation distance.

4.2. Participants and apparatus

We recruited 8 participants (four males and four females, aged between 22 and 29, $M = 24.875$, $SD = 2.09$, all right-handed) with normal vision (or corrected-to-normal vision by wearing glasses). Six of them had experience using HMD VR applications before the study, and none reported balance disorders.

Our system used an HTC Vive Pro HMD powered by a workstation with a 3.8 GHz Intel(R) Core(TM) i7-10700KF CPU, 32 GB of RAM, an NVIDIA GeForce GTX 3080Ti graphics card, and an HTC Vive tracker. Before using the Vive tracker, we tested its positioning accuracy. We bound the tracker to the arm of a static mannequin with movable joints, which we posed in five poses and collected the position of the tracker for each pose over 5 min. The result position array of the tracker shows that the average distance between data from two adjacent positions sampled from the same pose was 1.2 cm (maximum 1.6 cm). The difference is smaller than the offset distance we set to the user's joints (from 4 cm to 6 cm, depending on the thickness of the user's joints). Therefore, the effect of the tracker noise is negligible. The whole system was running at 90 fps for each eye. Participants said they felt the presence of the belt holding the tracker in place, but their movement was not affected by the belt. Before each participant started the experiment, we measured the inter-pupillary distance (IPD) for them with a millimeter scale and adjusted the IPD of the headset to meet their best visual setting.

4.3. User study design

We designed a within-subjects virtual object-translating task. Participants were asked to translate six solid white spheres on the ground to the target locations (marked as green spheres) with specified precision, as shown in Fig. 5. According to Fitts' law (Graham and MacKenzie, 1996), there are trade-offs between accuracy and speed when manipulating objects. We set the precision to 0.02 m in the user study according to the observation in the informal test. The task will not be too challenging or too easy for the participants. Thus, the data collected could be general and can reveal the characteristics of the metaphor. There are eight target positions at different distances $d \in \{0.5\text{ m}, 1\text{ m}, 2\text{ m}, 3\text{ m}, 4\text{ m}, 5\text{ m}, 5.5\text{ m}, 6\text{ m}\}$ from the user. The maximum touch distance in the virtual environment D_m is set to 6.5 m. The design principle of the experimental scene is to ensure that the participants can complete a trial (translating one sphere to the target position) within 20 s anywhere in the reachable manipulation space.

4.4. Procedure and metric

In the first stage, we aim to fit the $t_2 - \beta$ model in Eq. (4). Eight participants were asked to translate the six spheres on the ground to the target positions with specified precision using our basic Big-Arm method. When the manipulated sphere is less than 0.02 m from the target, the system gives visual feedback to the user, turning the manipulated sphere red.

In order to determine the coefficients, we need to collect the user's real arm motion data precisely. We used three HTC Vive trackers, binding on the user's shoulder, elbow, and wrist joints. For each translation, we record the coarse approach time t_1 and the fine-tuning adjustment time t_2 of the six spheres, respectively, and calculate the average of t_1 and t_2. We also record the positions of the user's shoulder, elbow, and wrist with the three trackers and calculate the user's real elbow angle β when the user presses the button to end the t_2 stage. After all eight participants translated the spheres, we got 64 groups of measured data to fit the $t_2 - \beta$ model.

When the $t_2 - beta$ model is acquired, we complete the optimized EEBA method and start the second stage. To reduce the impact of the first stage, we commence the second stage tasks one week later. The eight participants repeated the same translating sphere task procedure using the EEBA method. The same time metrics (t_1 and t_2) are also collected. Then, we compare the performances of the two methods.

4.5. Results and discussion

For the fitting process, we plot the collected t_2 and β in the first stage of the pilot user study in Fig. 6 top, fit the model illustrated in Eq. (4) with the iterative least squares estimation method, and get the coefficients $\{e_i | i = 1, 2, \ldots, 7\} = \{0.79, -2.48, 2.27, -23.95, 1.66, 1.84, 29.12\}$. The resulting mapping curve is shown in orange in Fig. 6 top. When the t_2 time reaches its minimum value, the corresponding real elbow angle β is around 90 degrees. When β deviates from 90 degrees, the t_2 time increases. The fitted model was consistent with our empirical assumptions. We can use the fitted model to calculate the optimized elbow angle mapping function with Eq. (5). Coefficients a and b can be calculated with Eq. (6). Fig. 6, bottom shows one example of the mapping function, with the coefficients $a = 2.85, b = 0.06$, $\beta_{max} = \beta'_{max} = 150°$, $\beta_{min} = 50°$. β'_{min} is calculated with Eq. (1): third row. The derivative function of this curve is proportional to the reciprocal function of the top curve.

In the second stage of the pilot user study, we compare the performances of the basic Big-Arm and the optimized EEBA method. The average t_1 and t_2 results for the two methods are shown in Fig. 7. We analyzed the data with the one-way Repeated Measures ANOVA. For the coarse approaching time t_1 (blue and gray bars), the EEBA method performs better at all distances, and the ANOVA results reveal a statistically significant difference ($F(1.0, 7.0) = 17.184, p = 0.004, \eta^2 = 0.711$). A post-hoc analysis shows t_1 for the EEBA method ($M = 2.19, SD = 0.25$) is significantly ($p = .014$) lower than that for the basic Big-Arm method ($M = 2.73, SD = 0.48$). The results support **H0-a**. We believe it is because the β range for EEBA [50°,150°] is smaller than the range for the basic Big-Arm, which means when participants rotate their elbows at the same angle, the object sphere moves more. So, the overall translating speed of the virtual spheres becomes faster.

We also compare the fine-tuning adjusting time t_2 (orange and yellow lines) for the basic Big-Arm and EEBA methods. The ANOVA test shows that there was no significant difference across the eight distances ($F(1.0, 7.0) = 0.981, p = 0.355, \eta^2 = 0.123$). We ran the Repeated Measure ANOVA test on the experiment data to validate the second hypothesis when target distance $d = 6$ m. The results show a statistically significant

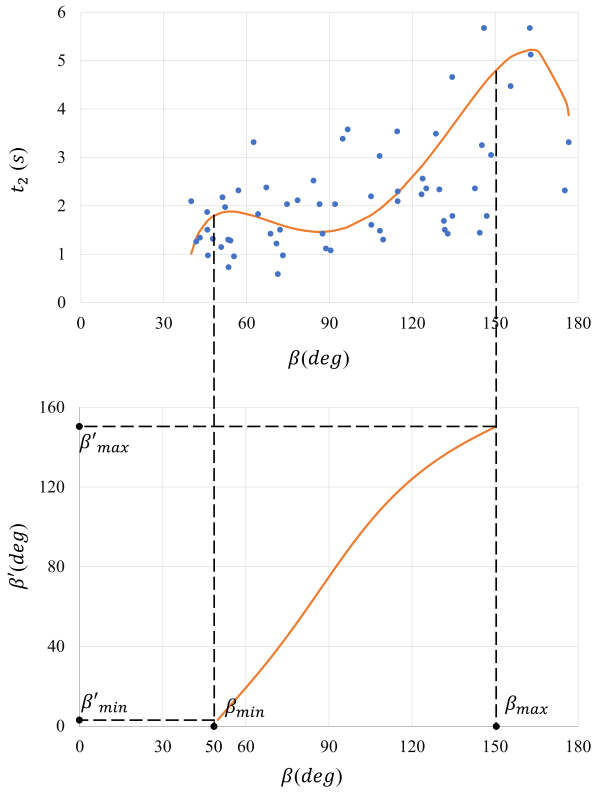

Fig. 6. The top row shows the fitted curve of the model in Eq. (4). The bottom row shows an example of the optimized mapping function.

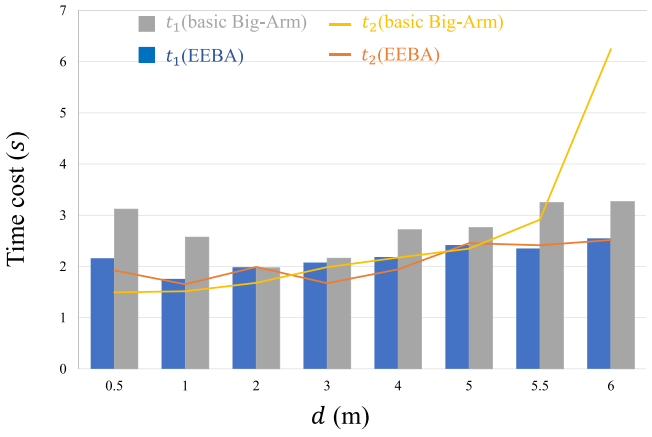

Fig. 7. t_1 and t_2 time cost with the basic Big-Arm and the EEBA methods for different target distances (d).

difference ($F(1.0, 7.0) = 7.346, p = 0.03, \eta^2 = 0.512$). A post hoc analysis shows that when the target distance is 6 m, t_2 for the EEBA method ($M = 2.52, SD = 0.84$) is significantly ($p = .018$) lower than that for the basic Big-Arm method ($M = 6.24, SD = 1.37$). The figure shows a more gentle and uniform t_2 time across the manipulation space. The results support **H0-b**.

5. User study 1: Ergonomic validation

5.1. Overview and hypotheses

After finishing the model fitting, we acquired and applied the EEBA method to the context of the target selection task. We aimed to validate that the proposed EEBA method can increase comfort during manipulation. Thus, we formulate the following hypotheses:

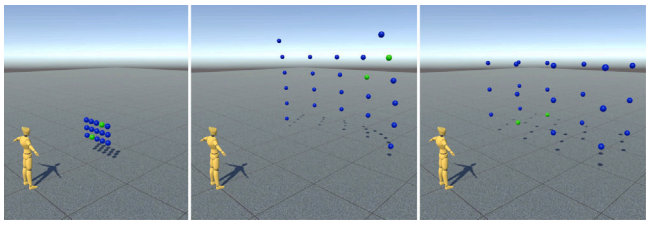

Fig. 8. The *Ergonomic* (left), *Limits* (middle), and *Fixed* (right) sphere layouts with D_m=6 m. The target pair of spheres are highlighted in green.

H1. The EEBA method can increase comfort for selecting objects near the manipulation space boundary.

H2. It takes less time for users to finish the selection task with the EEBA method.

5.2. Participants and apparatus

We recruited 16 participants (none of them participated in the last user study), eight males and eight females between 21 and 29 years old ($M = 24.375$, $SD = 2.12$), with normal vision (or corrected-to-normal vision by wearing glasses). Six have experience using HMD VR applications, and none reported balance disorders.

The system set up for this user study is the same as the system used for the pilot user study. Also, we use three HTC Vive trackers bound on the participant's shoulder, elbow, and wrist and a handheld controller to track the physical arm pose for further data analysis. Participants reported their motion was not affected by the trackers and belts. Before each participant started the experiment, we measured their IPD data and adjusted the HMDs to meet their best setting. The whole system was running at 90fps for each eye.

5.3. User study design

We used a 3 × 3 × 3 repeated measures within-subjects design. The user study refers to the basic setting of the study used to evaluate Erg-O (Montano Murillo et al., 2017; Wentzel et al., 2020). We tested three manipulation methods (Go-Go (Poupyrev et al., 1996), Linear Offset (LO) (Li et al., 2018), and our EEBA) with three target layouts (ergonomic, limits of reach, and world fixed) and three maximum distances (D_m = 2 m, 6 m, and 10 m) in the target selection task.

Participants were asked to select the highlighted spheres as quickly as possible. At the beginning of the task, several blue spheres (15 to 24) were floated in front of the participants. Then, two spheres were randomly highlighted as green, and the participant selected the green spheres using the controller. Once the selection is correct, the green sphere turns back to blue, and then the system randomly highlights two more spheres as green for the participant to select, and the process is repeated 30 times. The accompanying video demonstrates this task.

Target Layouts The spheres were placed according to the three target layouts used in the Erg-O study (Montano Murillo et al., 2017): (1) with the *Ergonomic* layout, 15 spheres were placed in a 5 × 3 grid, $0.4D_m$ away from the participant's torso, on the *Center* and *Bent* plane (Hincapié-Ramos et al., 2014). (2) with the *Limits* layout, 24 spheres were placed in front of the participant, distributed on a spherical surface with a radius of D_m, a pitch of 30°, and a yaw of 60°. (3) with the *Fixed* layout, 24 spheres were placed in two 4 × 3 grids (one $0.3D_m$ away, the other $0.9D_m$ away), spanning across the entire reachable space of the virtual big arm ($D_m \times 0.6D_m \times 0.6D_m$). Detailed layout setting is shown in Fig. 8.

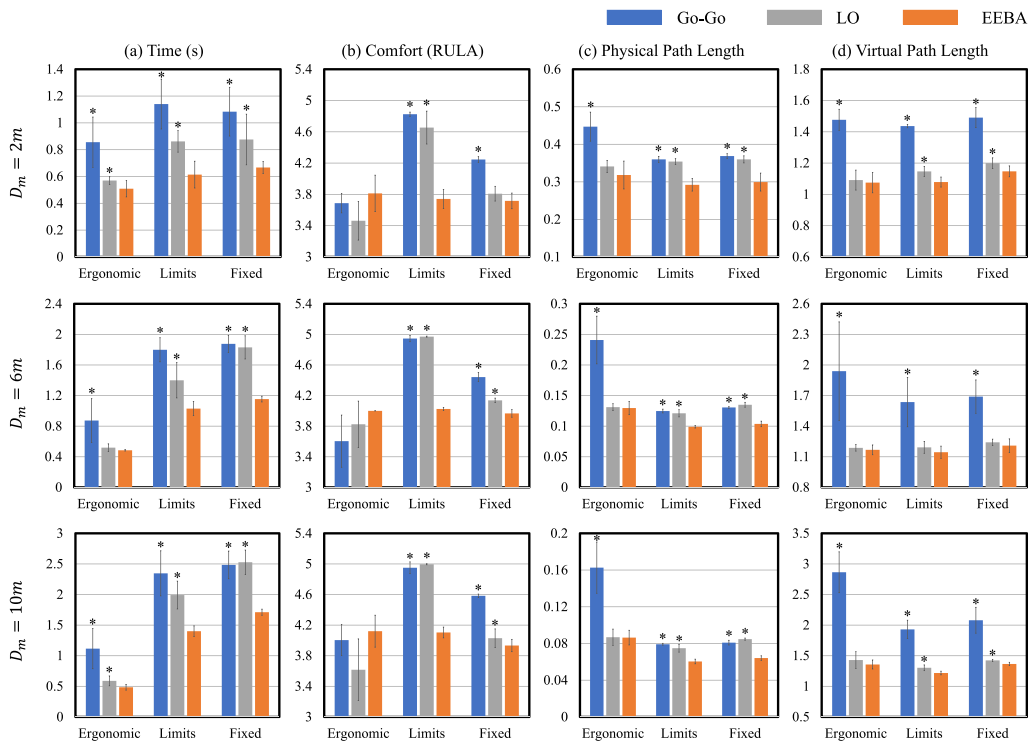

Fig. 9. (a) *Time*, (b) *Comfort*, (c) *Physical Path Length*, and (d) *Virtual Path Length* by *METHOD*, *LAYOUT* and D_m. Error bars are standard deviations. Significant differences are denoted with asterisks (all compared to the EEBA methods).

5.4. Procedure and metrics

This user study has three independent variables: *METHOD* with three types (*Go-Go*, *Linear Offset*, *EEBA*), *LAYOUT* with three levels (*Ergonomic*, *Limits*, *Fixed*) and D_m with three levels (2 m, 6 m, 10 m). Each participant completed a 27-condition task (all combinations of the three variables) according to the order of the *METHOD* determined by the balanced Latin square. Each condition contained 30 trials.

The performance of all participants was quantified with the following objective metrics: *Time*, *Comfort*, *Physical Path Length*, and *Virtual Path Length*, the same as Montano Murillo et al. (2017), Wentzel et al. (2020). *Time* is the period of a trial-selecting the first and second highlighted target spheres. *Comfort* is measured with the RULA score of the ergonomic measurement system (McAtamney and Corlett, 1993). When selecting the target sphere, we recorded the participant's shoulder, elbow, and wrist positions to calculate the RULA score. The lower the RULA score, the lower the participant's exposure to ergonomic risk factors. *Physical Path Length* (or *Virtual Path Length*) is the ratio of the traveling distance of the participant's physical hand (or virtual hand) divided by the distance between two highlighted target spheres.

After each condition, we asked the participant to self-report the *comfort*, *ease of reach*, *overstretching*, and *sense of control* on a scale from 1 to 7, the same as that in the Erg-O study (Montano Murillo et al., 2017).

5.5. Results

For each participant and each condition, the outliers of the 30 trial data points were first filtered out (±3 standard deviation). In total, we removed 416 trials (3.2%). The distribution normality assumption was verified using the Shapiro–Wilk test.

In the following analysis, we applied a two-way repeated measures ANOVA with Holm–Bonferroni corrected post-hoc pairwise t-test unless noted otherwise. We verified that sphericity (Mauchly test) was not violated with any measures. The results are shown in Fig. 9 and Appendix A.

5.5.1. Time

Fig. 9, column (a) and Table A.3 give the *Time* metric results. The main effects of *METHOD* on *Time* is statistically significant, spheticity assumed $F(2,42) = 123.46, p < .001, \eta_p^2 = 0.86$. This effect was qualified by a significant $METHOD \times D_m$ interaction effect ($F(4,42) = 3.89, p = .011, \eta_p^2 = .27$) and a significant $METHOD \times LAYOUT$ interaction effect ($F(4,42) = 49.79, p < .001, \eta_p^2 = .70$). The result of post-hoc pair-wise comparisons shows that the EEBA method reduces the time cost significantly ($p < .032$) except for one condition ($LAYOUT = Ergonomic, D_m = 6$ m), under which the time reduction (6.6%) is not significant ($p = .097$) compared with the LO method.

5.5.2. Comfort (RULA)

Fig. 9, column (b) and Table A.4 show the results of the *Comfort* metric. The main effects of *METHOD* on *Comfort* is statistically significant, spheticity assumed $F = (2,42) = 103.66, p < .001, \eta_p^2 = .83$. This effect was qualified by a significant $METHOD \times D_m$ interaction effect ($F(4,42) = 4.66, p = .02, \eta_p^2 = .31$) and a significant $METHOD \times LAYOUT$ interaction effect ($F(4,42) = 77.63, p < .001, \eta_p^2 = .79$). The result of pair-wise comparisons shows that for layout *Limits*, the EEBA method reduces the RULA scores significantly (all $p < .001$), which means better comfort performance. For layout *Fixed*, the EEBA method reduces the RULA scores significantly ($p < .001$) except for two conditions ($D_m = 2$ m, $METHOD = LO, p = 0.1$ and $D_m = 10$ m, $METHOD = LO, p = 0.11$) However, for layout *Ergonomic*, the EEBA method increases the RULA scores.

5.5.3. Physical Path Length

Fig. 9, column (c) and Table A.5 show the results of the *Physical Path Length* metric. The main effects of *METHOD* on *Physical Path Length* is statistically significant, spheticity assumed $F = (2,42) = 328.04, p < .001, \eta_p^2 = .94$. This effect was qualified by a significant $METHOD \times D_m$ interaction effect ($F(4,42) = 22.51$,p< $0.001, \eta_p^2 = .68$) and a significant $METHOD \times LAYOUT$ interaction effect ($F(4,42) = 109.39, p < .001, \eta_p^2 = .84$). The result of pair-wise comparisons shows

Table 2
Pairwise Wilcoxon signed-rank test results for self-report metric. Asterisks denote statistical significance.

Question	Method	Avg. ± std.	Z	p
Comfort	Go-Go	4.06 ± 1.00	−6.51[a]	<0.001*
	LO	4.32 ± 0.94	−5.58[a]	<0.001*
	EEBA	5.10 ± 0.75		
Ease of Reach	Go-Go	4.03 ± 1.17	−6.80[a]	<0.001*
	LO	4.68 ± 1.21	−5.30[a]	<0.001*
	EEBA	5.29 ± 0.82		
Overstretching	Go-Go	4.42 ± 0.88	−6.52[b]	<0.001*
	LO	3.75 ± 1.36	−5.27[b]	<0.001*
	EEBA	3.03 ± 0.99		
Sense of Control	Go-Go	3.79 ± 1.10	−6.26[a]	<0.001*
	LO	4.13 ± 1.19	−4.92[a]	<0.001*
	EEBA	4.78 ± 1.11		

[a] Based on negative ranks.
[b] Based on positive ranks.

that the EEBA method reduces the *Physical Path Length* significantly ($p < .011$) except for three conditions ($LAYOUT = Ergonomic, D_m = 2m \& LAYOUT = Ergonomic, D_m = 6m \& LAYOUT = Ergonomic, D_m = 10m$), under which the reduction (6.7% & 1.12% & 0.48%) is not significant ($p = .16 \& p = .76 \& p = .93$) compared with the LO method.

5.5.4. Virtual Path Length

Fig. 9, column (d) and Table A.6 shows the results of the *Virtual Path Length* metric. The main effects of *METHOD* on *Virtual Path Length* is statistically significant, spheticity assumed $F = (2, 42) = 248.79, p < .001, \eta_p^2 = .92$. This effect was qualified by a significant $METHOD \times D_m$ interaction effect ($F(4, 42) = 19.83$,p< $0.001, \eta_p^2 = .65$) and a significant $METHOD \times LAYOUT$ interaction effect ($F(4, 42) = 36.30, p < .001, \eta_p^2 = .63$). The result of pair-wise comparisons shows that compared to the Go-Go method, the EEBA method reduces the *Virtual Path Length* significantly for all conditions ($p < .001$). Compared to the LO method, the reducing effects show significant reductions ($p < .013$) when $LAYOUT \in Limits, Fixed \& D_m \in 2$ m, 10 m. For other conditions, the reductions are not significant.

5.5.5. Self-report

Table 2 shows the results of the self-report questionnaire for each measure. Pairwise Wilcoxon signed-rank tests found the EEBA method shows statistically significant improvements compared to the Go-Go and LO methods.

5.6. Discussion

The primary goal of this user study is to collect data for evaluating the comfort performance of our EEBA method relative to the Go-Go and LO methods. According to the results, the proposed EEBA method shows comparable performance and provides statistically significant improvements in comfort for *Limits* and *Fixed* layouts.

5.6.1. Time

For all conditions, the EEBA method reduces trial times. The reductions are apparent for *Limits* and *Fixed* layouts. We believe it is because the participants with our EEBA method can easily pre-plan the translating path and control the movement of the virtual hand. On the other hand, due to the newly mapped smaller elbow angle range, the participants can translate the virtual hand for a certain distance with lesser physical arm movement, leading to faster manipulation and less trial time. The *Time* metric results support **H2**.

When D_m increases from 2 m to 10 m, the trial time increases for both *Limits* and *Fixed* layout, while the increase is not apparent for *Ergonomic* layout. For *Limits* and *Fixed*, when D_m increases, the distances between the sphere and the target location also increase. However, the distances for *Ergonomic* layout stay the same. Since the sphere's size remains the same, the *Time* and Index of Difficulty (ID) of the tasks exhibit a proportional relationship with the value of D_m, confirming that the experimental results adhere to Fitts' Law.

5.6.2. Comfort

For *Limits* and *Fixed* layouts, our EEBA method reduces the RULA scores significantly. However, for *Ergonomic* layout, the RULA scores of our EEBA method are larger compared to the Go-Go and LO methods. The EEBA's optimized mapping function readjusts the elbow angle to the new range [50°, 150°]. This design avoids the extreme arm extension pose for the target sphere in the *Limits* layout, thus increasing the comfort. This result supports **H1**. For *Fixed* layout, the RULA scores of our EEBA method are also lower, which indicates better comfort for target spheres whose positions are placed throughout the reachable space. Regarding the *Ergonomic* layout, our EEBA method yields higher scores. Our EEBA method is more suitable for distant object manipulation. The RULA scores of all three methods in the *Ergonomic* layout are much smaller than the other two, meaning the participants are more comfortable in this distance range. However, our EEBA method has higher RULA values than the other two. As a result, our EEBA approach reduces the comfort level in close-range manipulation in exchange for a significant increase in distant object manipulation.

5.6.3. Physical Path Length

The general reduction for all conditions verifies that our EEBA method can reduce physical movements. This is caused by the smaller real mapping elbow angle range illustrated in Section 3.2.1. The same virtual hand movement requires less physical hand movement.

5.6.4. Virtual Path Length

The reduction shows that the participants can better control virtual hand movements with the EEBA method. We attribute the reduced virtual path length to the intuitive path pre-planning and familiar virtual arm control.

5.6.5. Self-reports

The responses regarding the four metrics are more favorable for our EEBA method than the Go-Go and LO methods. The improvement effects are significant, which shows better comfort performance and adaptability of the proposed EEBA method in VR.

6. User study 2-efficiency evaluation

6.1. Overview and hypotheses

The second user study aims to explore the efficiency performance of our EEBA method. In this study, we investigated the influence of various factors on target translating performance. We formulate the following hypotheses:

H3. The EEBA method can reduce the translating time during the coarse approaching phase.

H4. The EEBA method can reduce the adjusting time during the fine-tuning phase.

6.2. Participants and apparatus

We recruited 16 participants, eight males, and eight females (none participated in the last two user studies), ranging from 20 to 30 years old ($M = 23.69$, $SD = 2.31$), with normal vision (or corrected-to-normal vision by wearing glasses). Thirteen had used immersive HMD VR applications before, and none reported balance disorders.

The system setup is the same as in the previous user studies. In this user study, only one tracker is used to capture the elbow joint position. No participant reported being uncomfortable with the tracker. Before each participant started the experiment, we measured their IPD data and adjusted the HMDs to meet their best setting. The whole system was running at 90 fps for each eye.

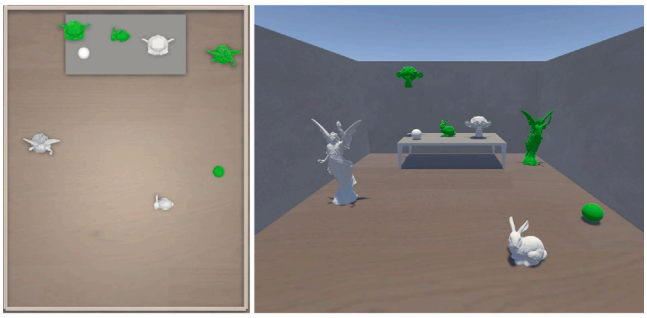

Fig. 10. The indoor VR room used in user study 2 for D_m=6 m. The left figure shows the top view and the right figure shows the view of the participant. The rooms used for D_m = 2 m and D_m=10 m have similar layouts but different sizes. Please refer to the accompanying video.

6.3. User study design

We used a 4 × 3 × 3 repeated measures within-subject design. The task for the participants is to translate four white virtual objects (sphere, bunny, monkey, and Lucy statue) to their target locations (highlighted as green) within particular precision in three indoor VR rooms of different sizes (Fig. 10). The three rooms' furthest object (monkey) distances are 1.92 m, 5.76 m, and 9.87 m.

We compared four methods: Ray-casting (RC) (Bowman and Hodges, 1997), Go-Go (Poupyrev et al., 1996), LO (Li et al., 2018), and EEBA method, under three max distance conditions (D_m=2 m, 6 m, and 10 m) with three precision requirements ($prec.$ = 0.05 m, 0.03 m, and 0.02 m).

Participants were told to translate these objects to their target locations within three specified precision requirements as quickly as possible. When the distances between the objects and their targets are smaller than the precision value, the objects' color changes to red. Then participants can press a button to place the objects. After all four objects are successfully placed, the task is complete. If participants could not successfully place the objects, they were allowed to give up after several attempts.

6.4. Procedure and metrics

This user study has three independent variables: *METHOD* with four types (RC, Go-Go, LO, EEBA), *PRECISION* with three levels (0.05 m, 0.03 m, 0.02 m) and D_m with three levels (2 m, 6 m, 10 m). Each participant completed all combinations of the three variables, with the order of *METHOD* determined by a balanced Latin square.

The task is completed when all four objects are placed in their target locations. The performance was quantified with four objective metrics: t_1, t_2, *Approach Path Length*, and *Fine-tuning Length*. t_1 is the total time cost for all four objects during the approaching stage. t_2 is the total time cost for all four objects during the final position adjustment stage. t_1 and t_2 for each object are collected the same way as in Section 4. *Approach Path Length* is the ratio of the total length of the virtual object trajectories during the coarse approaching stage for the four objects, divided by the total distance between the four objects and their corresponding target locations. *Fine-tuning Length* is the total absolute length of the virtual object trajectories during the fine-tuning stage for the four objects.

We also evaluated the user task load and usability performance with the standard NASA TLX questionnaire (Hart, 2006; Hart and Staveland, 1988), and various aspects of usability measured with the usability questionnaire (Kim et al., 2015). When participants completed one condition, they were asked to complete the questionnaires.

We filtered the data with three times the standard deviation and removed 12 (2.1%) outliers. The distribution normality assumption was verified using the Shapiro–Wilk test. Then, we analyzed the data with a two-way repeated measures ANOVA with Holm–Bonferroni corrected post-hoc pairwise t-test unless noted otherwise. We verified that sphericity (Mauchly test) was not violated with any measures. Fig. 11 and Appendix B gives the results for the four methods.

6.5. Results

6.5.1. t_1 time

Fig. 11, column (a) and Table B.7 give the t_1 metric results. The main effects of *METHOD* on t_1 is statistically significant, spheticity assumed $F(3,63) = 660.02, p < .001, \eta_p^2 = .97$. The main effects of *PRECISION* on t_1 is also statistically significant, spheticity assumed $F(2,42) = 149.45, p < .001, \eta_p^2 = .88$. The effects were qualified by a significant *METHOD* $\times D_m$ interaction effect ($F(6,63) = 145.86, p < .001, \eta_p^2 = .93$), a significant *PRECISION* $\times D_m$ interaction effect ($F(4,42) = 100.94, p < .001, \eta_p^2 = .91$) and a significant *PRESISION* × *METHOD* interaction effect ($F(6,63) = 94.29, p < .001, \eta_p^2 = .82$).

The result of post-hoc pairwise comparisons shows that compared to the RC method, the EEBA method reduces t_1 time significantly for all precision and D_m levels ($p < .001$). Compared to the Go-Go method, for D_m = 6 m and D_m = 10 m, the EEBA method shows significant t_1 reductions ($p < .026$). However, for D_m = 2 m, the reduction is not statistically significant when the precision level equals 0.03 m ($p = .28$). When the precision level equals 0.05 m and 0.02 m, the result shows significant reductions ($p < .001$). Compared to the LO method, the EEBA method reduces the t_1 time significantly ($p < 0.03$) except for conditions ($PRECISION = 0.03, D_m = 2$ m, $p = .54$, $PRECISION = 0.05, D_m =$ 10 m, $p = .145$ and $PRECISION = 0.02, D_m = 10$ m, $p = .07$).

6.5.2. t_2 time

Fig. 11, column (b) and Table B.8 give the t_2 metric results. The main effects of *METHOD* on t_2 is statistically significant, spheticity assumed $F(3,63) = 164.47, p < .001, \eta_p^2 = .89$. The main effects of *PRECISION* on t_2 is also statistically significant, spheticity assumed $F(2,42) = 214.90, p < .001, \eta_p^2 = .91$. The effects were qualified by a significant *METHOD* $\times D_m$ interaction effect ($F(6,63) = 64.44, p < .001, \eta_p^2 = .86$), a significant *PRECISION* $\times D_m$ interaction effect ($F(4,42) = 98.82, p < .001, \eta_p^2 = .90$) and a significant *PRESISION* × *METHOD* interaction effect ($F(6,63) = 23.80, p < .001, \eta_p^2 = .53$).

The post hoc pairwise comparison results show that the EEBA method reduces t_2 time significantly ($p < 0.03$) except for conditions ($PRECISION = 0.05$ m, $D_m = 6$ m, $p = 0.35$ and $PRECISISON = 0.03, D_m = 6$ m, $p = 0.15$). Compared to the Go-Go method, the EEBA method reduces t_2 time significantly for all precision and D_m levels ($p < .003$). Compared to the LO method, the EEBA method significantly ($p < .002$) reduces the t_2 time when D_m = 6 m and D_m = 10 m. When D_m = 2 m, the t_2 time reductions of our EEBA method are not significant when the precision level equals 0.05 m ($p = .77$) and 0.03 m ($p = .06$). The reduction is significant when the precision level reaches 0.02 m ($p = .002$).

6.5.3. Approach Path Length

Fig. 11, column (c) and Table B.7 give the *Approach Path Length* metric results. The main effects of *METHOD* on *Approach Path Length* is statistically significant, spheticity assumed $F(3,63) = 463.39, p < .001, \eta_p^2 = .96$. The main effects of *PRECISION* on *Approach Path Length* is also statistically significant, spheticity assumed $F(2,42) = 11.30, p < .001, \eta_p^2 = .35$. The effects were qualified by a significant *METHOD* $\times D_m$ interaction effect ($F(6,63) = 51.68, p < .001, \eta_p^2 = .83$), a significant *PRECISION* $\times D_m$ interaction effect ($F(4,42) = 18.28, p < .001, \eta_p^2 = .64$) and a significant *PRESISION* × *METHOD* interaction effect ($F(6,63) = 45.04, p < .001, \eta_p^2 = .68$).

The post hoc pairwise comparison results show that the EEBA method reduces *Approach Path Length* significantly for all precision and D_m levels ($p < .001$) compared to the RC and the Go-Go method. Compared to the LO method, the EEBA method significantly ($p < .028$) reduces *Approach Path Length* except for conditions ($PRECISION =$

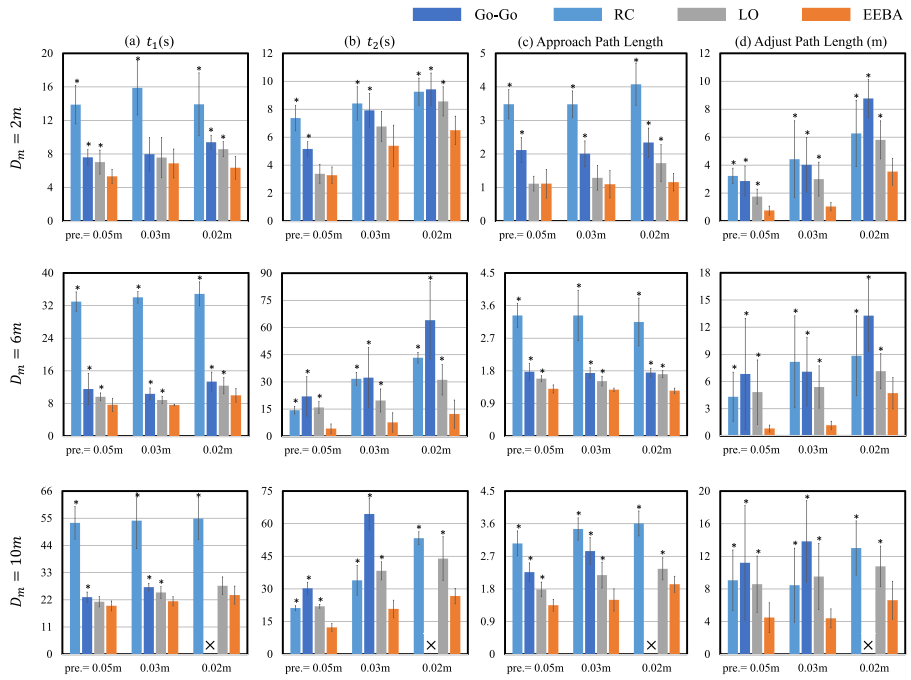

Fig. 11. (a) t_1, (b) t_2, (c) *Approach Path Length (APL)*, and (d) *Fine-tuning Path Length (FPL)* by *METHOD*, *PRECISION* and D_m. Error bars are standard deviations. Significant differences are denoted with asterisks (all compared to the EEBA methods). The × mark indicates the task is not completed under the corresponding condition.

0.05 m, D_m = 2 m, p = 0.99 and $PRECISISON$ = 0.03, D_m = 2 m, p = 0.37).

6.5.4. Fine-tuning Path Length

Fig. 11, column (d) and Table B.7 give the *Fine-tuning Path Length* metric results. The main effects of *METHOD* on *FPL* is statistically significant, spheticity assumed $F(3,63) = 44.82, p < .001, \eta_p^2 = .68$. The main effects of *PRECISION* on *FPL* is also statistically significant, spheticity assumed $F(2,42) = 10.16, p = .001, \eta_p^2 = .33$. The effects were qualified by a significant *METHOD* ×D_m interaction effect ($F(6,63) = 4.84, p = .004, \eta_p^2 = .32$), a significant *PRECISION* ×D_m interaction effect ($F(4,42) = 5.18, p = .005, \eta_p^2 = .33$). While the *PRECISION* × *METHOD* interaction effect is not significant ($F(6,63) = 2.03, p = .12, \eta_p^2 = .09$).

The post hoc pairwise comparison results show that the EEBA method reduces *FPL* significantly for all precision and D_m levels ($p <$ .038) compared to the other three methods.

6.5.5. Task load and usability

Fig. 12 shows the task load scores for all conditions. The overall ANOVA test reveals significant differences between the four methods ($F(3,69) = 36.71, p < .001, \eta_p^2 = .62$). Post-hoc analysis reveals that the task load of the EEBA method is significantly smaller than that of the RC, Go-Go, and LO methods.

Fig. 13 shows the results in terms of usability perception. Detailed scores are presented, including *Intuitive* (IN), *Effective* (EF), *Accuracy* (AC), *Naturalness* (NA), *Satisfaction* (SA), and *Easiness* (EA).

For IN, The overall ANOVA test reveals significant differences between the four methods ($F(3,69) = 11.60, p < .001, \eta_p^2 = .59$). Post-hoc analysis reveals that the EEBA method shows overall improvements in all detailed scores. The improving effects are statistically significant ($p <$ .024), except for NA scores on the Go-Go (p = .09) and LO (p = .42) methods, SA score on the LO (p = .20) method and EA on the LO (p = .16) method.

6.6. Analysis and discussion

The results show that the proposed EEBA method shows significant improvements in efficiency compared to the RC, Go-Go, and LO methods.

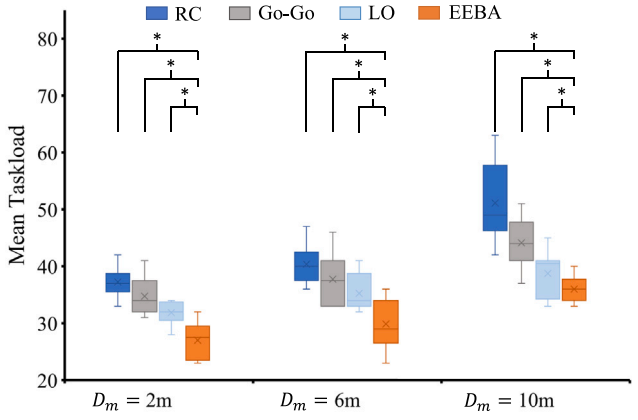

Fig. 12. Box plots for task load scores of the four methods and three D_m values. Asterisks denote statistical significance.

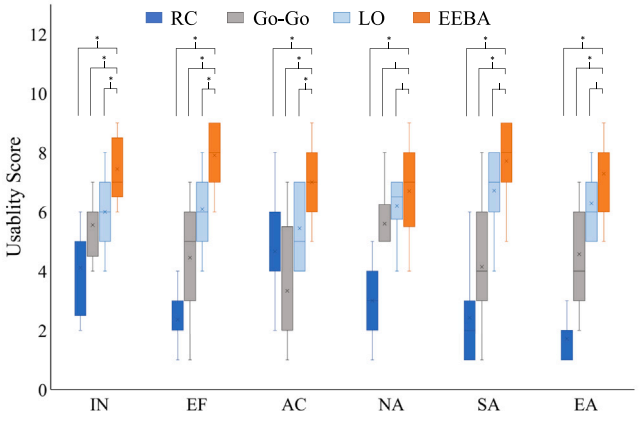

Fig. 13. Detailed usability subscores for the four methods. Compared with the EEBA, significant differences are denoted with asterisks.

6.6.1. t_1 time and Approach Path Length

From the results of t_1 and *Approach Path Length*, our EEBA method has a shorter virtual object translating trajectory, which we attribute to the fact that the participant's expected results for his actual manipulation are similar to those produced by our method, and his perceived translating in the virtual space is more consistent with his actual translating, thus consuming less time and manipulating more efficiently. At the same time, the newly mapped smaller elbow angle range enables a faster approach speed and less t_1 time. This result supports **H3**.

6.6.2. t_2 time and Fine-tuning Path Length

From the t_2 and *Fine-tuning Path Length* results, our EEBA method significantly improves the efficiency performance, especially for large scenarios. We believe the reason for the improvements is as follows. First, the proposed EEBA method allows participants to control the target's movement in relatively more ergonomic arm poses with low fatigue, making the adjustment sustainable. On the other hand, the link structure of the virtual arm functions the same way as the real arm, and participants can easily predict the reflected virtual hand movement of their controlling moves, leading to effective manipulation. The reduced t_2 time supports **H4**.

6.6.3. Task load and usability

Our EEBA method's lower task load score is due to its ergonomic improvement, provided by the optimized elbow angle mapping function. Participants can reach all the target objects distributed around the reachable space with a relatively comfortable arm pose, making their arms less prone to fatigue. We believe the increased usability scores are due to the EEBA method's intuitive arm-like structure. Participants felt that it was easy to understand how to use it.

6.6.4. Discussion

We also believe that proprioception is one of the reasons for the better performance of our method. When the user controls their physical arm to extend or bend, the virtual arm reflects the same motions. Due to the similarity between the virtual arm and the physical arm motion, the signals detected by the proprioceptors (located within muscles, tendons, and joints) will be integrated with image frames of virtual arm motion captured by the visual sensory. This mechanic offers human-like control feedback, and it will strengthen confidence and easiness when operating the virtual target object.

7. Conclusion, limitations, and future work

We have proposed an efficient and ergonomic Big-Arm metaphor for manipulating distant objects in VR. Our method prolongs the arm limbs and maps the real and virtual elbow angles with an optimized elbow angle mapping function fitted from a pilot user study. We also evaluate the performance of our EEBA method in two subsequent user studies. Compared to the state-of-the-art methods, the proposed EEBA method proved more efficient and ergonomic in distant virtual object manipulation tasks. Furthermore, according to the perception questionnaire, our EEBA method shows better task load and usability performance.

Our approach facilitates full-range object manipulation within the virtual arm's reachable distance. Employing an optimized elbow angle mapping technique, we enhance and equalize the user's efficiency in object manipulation. In essence, our method enables users to easily manipulate scattered target objects in the scene without needing to relocate. It is important to note that while the arm's length is not infinitely extendable, excessively long arms may compromise maneuverability. For expansive scenes, our method can be supplemented with existing user relocation techniques. By adopting our approach, users benefit from an extended operating range, reducing the need for frequent relocating and thereby enhancing operational efficiency and reducing workload within the scene.

Besides, our EEBA method supports easy and direct selection and translation and can be easily integrated with common rotation. A simple implementation is conducted by mapping the rotation operation with the controller's rotation. Please refer to the accompanying video for details and intuitive effects. In future work, we plan to delve deeper into investigating the impact of the EEBA method on rotational manipulation, further enhancing our understanding of its comprehensive usability. Our method is better suited for fast object placement in large scenes. This is especially true for scenes where objects exist to move across significant depths. The method is also suitable for manipulating objects floating in mid-air because the linkage design, like a real arm, allows the user to quickly construct the motion path of a virtual hand approaching an object in the air.

One limitation of our method is that we use a tracker to track users' elbows accurately. Before implementing the system with a tracker, we also implemented the EEBA method for user arm motion estimation based on inverse kinematics (Parger et al., 2018), which does not require any additional tracker but does not perform robustly in user study (please refer to the accompanying video). This also shows that our EEBA method can be very easily integrated with feasible arm-tracking systems. Future work could consider integrating more stable and feasible arm-tracking methods (Spanlang et al., 2010; Jiang et al., 2016; Winkler et al., 2022; Yi et al., 2022). The limited participant count in our user studies poses a challenge, particularly given the multitude of conditions examined. To address this limitation in future research, employing G-power to estimate the necessary participant numbers will enhance the robustness and validity of our findings.

Another limitation is that we currently check the participants' mobility by asking them directly. However, such questioning only provides subjective feedback and does not provide objective corroboration that the arm mobility is similar for each participant. The final limitation pertains to the current display of the virtual arm, which is partially obscured by the floor. We tried the transparent display of the obscured part of the arm in the pre-design phase. However, from some participants' feedback, they were disturbed to various degrees, so we abandoned the transparent scheme. Of course, our preliminary transparency scheme is just a simple test. In future work, many available schemes, such as changing transparency, color changing of the occluded part, coloring according to the depth of the arm position, etc., are worth trying.

Another future work could extend our EEBA metaphor in augmented reality by wearing a haptic glove. This glove allows the user to manipulate the distant virtual object in the mixed environment and gives the user haptic feedback when he/she touches the distant real object.

CRediT authorship contribution statement

Jian Wu: Conceptualization, Formal analysis, Methodology, Resources, Software, Visualization, Writing – original draft, Writing – review & editing. **Lili Wang:** Conceptualization, Funding acquisition, Investigation, Methodology, Project administration, Resources, Supervision, Visualization, Writing – original draft, Writing – review & editing. **Sio Kei Im:** Conceptualization, Investigation, Methodology, Supervision, Validation. **Chan Tong Lam:** Investigation, Methodology, Supervision.

Declaration of competing interest

The authors declare that they have no known competing financial interests or personal relationships that could have appeared to influence the work reported in this paper.

Data availability

Data will be made available on request.

Acknowledgments

This work was supported by the National Natural Science Foundation of China through Projects 61932003 and 62372026, by Beijing Science and Technology Plan Project Z221100007722004, by National Key R&D plan 2019YFC1521102.

Appendix A. Detailed test results for User Study 1

Tables A.3, A.4, A.5, and A.6 show the detailed results of the User Study 1. In addition to a two-way repeated measures ANOVA with Holm–Bonferroni corrected posthoc pairwise t-test, we also quantified the effect size for each metric using Cohen's d (Cohen, 2013). The *d*

Table A.3
Time results for each condition. Asterisks denote statistical significance.

D_m	Layout	Method	Avg. ± std.	$(M_i - M_{EEBA})/M_i$	p	Cohen's d	Effect size
2 m	Ergonomic	Go-Go	0.86 ± 0.19	40.1%	< .001*	2.48	Huge
		LO	0.57 ± 0.03	10.73%	0.032*	1.28	Very Large
		EEBA	0.51 ± 0.06				
	Limits	Go-Go	1.14 ± 0.19	46.2%	< .001*	3.52	Huge
		LO	0.86 ± 0.08	28.8%	< .001*	2.72	Huge
		EEBA	5.10 ± 0.75				
	Fixed	Go-Go	1.08 ± 0.19	38.4%	< .001*	3.14	Huge
		LO	0.88 ± 0.19	23.9%	0.013*	1.52	Very Large
		EEBA	0.61 ± 0.1				
6 m	Ergonomic	Go-Go	0.87 ± 0.29	44.5%	0.003*	1.93	Very Large
		LO	0.52 ± 0.05	6.6%	0.097	0.95	Large
		EEBA	0.48 ± 0.01				
	Limits	Go-Go	1.80 ± 0.16	42.7%	< .001*	5.96	Huge
		LO	1.40 ± 0.23	26.5%	0.001*	2.10	Huge
		EEBA	1.03 ± 0.09				
	Fixed	Go-Go	1.88 ± 0.11	38.5%	< .001*	8.62	Huge
		LO	1.83 ± 0.15	36.9%	< .001*	6.09	Huge
		EEBA	1.15 ± 0.04				
10 m	Ergonomic	Go-Go	1.12 ± 0.33	56.6%	< .001*	2.69	Huge
		LO	0.59 ± 0.08	17.8%	0.01*	1.58	Very Large
		EEBA	0.48 ± 0.05				
	Limits	Go-Go	2.35 ± 0.37	40.3%	< .001*	3.52	Huge
		LO	1.99 ± 0.23	29.6%	< .001*	3.42	Huge
		EEBA	1.40 ± 0.09				
	Fixed	Go-Go	2.48 ± 0.23	31.1%	< .001*	4.70	Huge
		LO	2.53 ± 0.20	32.3%	< .001*	5.60	Huge
		EEBA	1.71 ± 0.05				

Table A.4
Comfort (RULA score) results for each condition. Asterisks denote statistical significance.

D_m	Layout	Method	Avg. ± std.	$(M_i - M_{EEBA})/M_i$	p	Cohen's d	Effect size
2 m	Ergonomic	Go-Go	3.69 ± 0.12	−3.39%	0.232	0.67	Medium
		LO	3.46 ± 0.25	−10.11%	0.017*	1.45	Very Large
		EEBA	3.81 ± 0.23				
	Limits	Go-Go	4.83 ± 0.03	22.5%	< .001*	12.28	Huge
		LO	4.65 ± 0.21	19.6%	< .001*	5.30	Huge
		EEBA	3.74 ± 0.12				
	Fixed	Go-Go	4.25 ± 0.04	12.5%	< .001*	7.00	Huge
		LO	3.81 ± 0.09	2.41%	0.10	0.94	Large
		EEBA	3.61 ± 0.1				
6 m	Ergonomic	Go-Go	3.60 ± 0.34	−11.0%	0.008*	1.64	Very Large
		LO	3.83 ± 0.30	−4.58%	0.15	0.82	Large
		EEBA	4.00 ± 0.00				
	Limits	Go-Go	4.95 ± 0.04	18.6%	< .001*	28.65	Huge
		LO	4.97 ± 0.01	19.0%	< .001*	66.94	Huge
		EEBA	4.03 ± 0.02				
	Fixed	Go-Go	4.44 ± 0.06	10.7%	< .001*	8.64	Huge
		LO	4.14 ± 0.03	4.1%	< .001*	4.15	Huge
		EEBA	3.97 ± 0.05				
10 m	Ergonomic	Go-Go	4.00 ± 0.20	−2.9%	0.31	0.57	Medium
		LO	3.62 ± 0.40	−13.9%	0.01*	1.57	Very Large
		EEBA	4.12 ± 0.21				
	Limits	Go-Go	4.95 ± 0.08	17.1%	< .001*	11.4	Huge
		LO	5.00 ± 0.01	17.9%	< .001*	17.65	Huge
		EEBA	4.10 ± 0.07				
	Fixed	Go-Go	4.58 ± 0.02	14.2%	< .001*	10.92	Huge
		LO	4.03 ± 0.12	2.38%	0.11	0.93	Large
		EEBA	3.93 ± 0.08				

Table A.5
Physical Path Length results for each condition. Asterisks denote statistical significance.

D_m	Layout	Method	Avg. ± std.	$(M_i - M_{EEBA})/M_i$	p	Cohen's d	Effect size
2 m	Ergonomic	Go-Go	0.45 ± 0.04	28.8%	< .001*	3.39	Huge
		LO	0.34 ± 0.02	6.7%	0.16	0.79	Medium
		EEBA	0.32 ± 0.04				
	Limits	Go-Go	0.36 ± 0.01	18.9%	< .001*	5.17	Huge
		LO	0.35 ± 0.01	17.5%	< .001*	4.76	Huge
		EEBA	0.29 ± 0.02				
	Fixed	Go-Go	0.37 ± 0.01	18.8%	< .001*	3.94	Huge
		LO	0.36 ± 0.01	16.8%	< .001*	3.30	Huge
		EEBA	0.30 ± 0.02				
6 m	Ergonomic	Go-Go	0.24 ± 0.04	46.2%	< .001*	3.88	Huge
		LO	0.13 ± 0.01	1.12%	0.76	0.17	Very Small
		EEBA	0.13 ± 0.01				
	Limits	Go-Go	0.12 ± 0.01	20.6%	< .001*	9.57	Huge
		LO	0.12 ± 0.01	18.2%	< .001*	4.96	Huge
		EEBA	0.09 ± 0.01				
	Fixed	Go-Go	0.13 ± 0.001	20.6%	< .001*	8.00	Huge
		LO	0.13 ± 0.004	23.1%	< .001*	7.27	Huge
		EEBA	0.10 ± 0.004				
10 m	Ergonomic	Go-Go	0.16 ± 0.03	46.9%	< .001*	3.71	Huge
		LO	0.087 ± 0.009	0.48%	0.93	0.05	Very Small
		EEBA	0.086 ± 0.008				
	Limits	Go-Go	0.08 ± 0.001	23.7%	< .001*	9.52	Huge
		LO	0.07 ± 0.004	19.32%	< .001*	4.06	Huge
		EEBA	0.06 ± 0.003				
	Fixed	Go-Go	0.08 ± 0.003	20.7%	< .001*	6.57	Huge
		LO	0.08 ± 0.001	24.3%	< .001*	10.49	Huge
		EEBA	0.06 ± 0.002				

Table A.6
Virtual Path Length results for each condition. Asterisks denote statistical significance.

D_m	Layout	Method	Avg. ± std.	$(M_i - M_{EEBA})/M_i$	p	Cohen's d	Effect size
2 m	Ergonomic	Go-Go	1.48 ± 0.07	27.2%	< .001*	6.05	Huge
		LO	1.09 ± 0.06	1.5%	0.65	0.25	Small
		EEBA	1.08 ± 0.06				
	Limits	Go-Go	1.44 ± 0.01	24.9%	< .001*	14.80	Huge
		LO	1.15 ± 0.03	5.9%	0.001*	2.16	Huge
		EEBA	1.08 ± 0.03				
	Fixed	Go-Go	1.49 ± 0.06	23.1%	< .001*	6.66	Huge
		LO	1.20 ± 0.03	4.4%	0.013*	1.53	Very Large
		EEBA	1.15 ± 0.03				
6 m	Ergonomic	Go-Go	1.94 ± 0.48	39.8%	< .001*	2.25	Huge
		LO	1.19 ± 0.03	1.6%	0.39	0.47	Small
		EEBA	1.17 ± 0.05				
	Limits	Go-Go	1.64 ± 0.24	30.0%	< .001*	2.79	Huge
		LO	1.19 ± 0.06	4.0%	0.15	0.81	Large
		EEBA	1.14 ± 0.06				
	Fixed	Go-Go	1.69 ± 0.16	28.4%	< .001*	3.84	Huge
		LO	1.24 ± 0.03	2.6%	0.27	0.62	Medium
		EEBA	1.21 ± 0.07				
10 m	Ergonomic	Go-Go	2.86 ± 0.33	52.6%	< .001*	6.23	Huge
		LO	1.43 ± 0.14	5.1%	0.24	0.66	Medium
		EEBA	1.36 ± 0.07				
	Limits	Go-Go	1.93 ± 0.15	36.9%	< .001*	6.58	Huge
		LO	1.30 ± 0.05	6.6%	0.001*	2.15	Huge
		EEBA	1.22 ± 0.03				
	Fixed	Go-Go	2.08 ± 0.21	34.4%	< .001*	4.72	Huge
		LO	1.42 ± 0.02	4.1%	< .001*	2.58	Huge
		EEBA	1.37 ± 0.03				

values were translated to qualitative effect size estimates of Huge ($d > 2.0$), Very Large ($2.0 > d > 1.2$), Large ($1.2 > d > 0.8$), Medium ($0.8 > d > 0.5$), Small ($0.5 > d > 0.2$), and Very Small ($0.2 > d > 0.01$). The statistical analysis was performed using the SPSS software (IBM, n.d.).

Appendix B. Detailed test results for User Study 2

Table B.7, Table B.8, Table B.9, and Table B.10 show the detailed results of the User Study 2. The same as Appendix A, in addition to a two-way repeated measures ANOVA with Holm–Bonferroni corrected posthoc pairwise t-test, we also quantified the effect size for each metric using Cohen's d (Cohen, 2013). The d values were translated to qualitative effect size estimates of Huge ($d > 2.0$), Very Large ($2.0 > d > 1.2$), Large ($1.2 > d > 0.8$), Medium ($0.8 > d > 0.5$), Small ($0.5 > d > 0.2$), and Very Small ($0.2 > d > 0.01$). The statistical analysis was performed using the SPSS software (IBM, n.d.).

Table B.7
t_1 results for each condition. Asterisks denote statistical significance.

D_m	Precision	Method	Avg. ± std.	$(M_i - M_{EEBA})/M_i$	p	Cohen's d	Effect size
2 m	0.05 m	RC	13.88 ± 2.30	61.7%	< .001*	4.95	Huge
		Go-Go	7.60 ± 0.92	30.0%	< .001*	2.59	Huge
		LO	7.03 ± 1.43	24.3%	0.02*	1.46	Very Large
		EEBA	5.32 ± 0.84				
	0.03 m	RC	15.88 ± 3.23	56.7%	< .001*	3.48	Huge
		Go-Go	7.98 ± 1.98	13.9%	0.28	0.60	Medium
		LO	7.57 ± 2.40	9.3%	0.54	0.34	Small
		EEBA	6.87 ± 1.73				
	0.02 m	RC	13.92 ± 3.76	54.5%	< .001*	2.69	Huge
		Go-Go	9.40 ± 0.83	32.6%	< .001*	2.73	Huge
		LO	8.58 ± 0.89	26.1%	0.003*	1.96	Very Large
		EEBA	6.34 ± 1.35				
6 m	0.05 m	RC	32.98 ± 2.38	76.8%	< .001*	12.43	Huge
		Go-Go	11.55 ± 3.84	33.8%	0.026*	1.33	Very Large
		LO	9.64 ± 0.95	20.7%	0.014*	1.50	Very Large
		EEBA	7.64 ± 1.62				
	0.03 m	RC	34.03 ± 1.43	77.6%	< .001*	25.86	Huge
		Go-Go	10.36 ± 1.45	26.6%	< .001*	2.66	Huge
		LO	8.85 ± 0.90	14.1%	0.003*	1.92	Very Large
		EEBA	7.61 ± 0.18				
	0.02 m	RC	34.87 ± 2.96	71.4%	< .001*	10.33	Huge
		Go-Go	13.36 ± 2.33	25.3%	0.008*	1.66	Very Large
		LO	12.36 ± 2.00	19.3%	0.03*	1.29	Very Large
		EEBA	9.97 ± 16.89				
10 m	0.05 m	RC	53.13 ± 6.59	63.2%	< .001*	6.89	Huge
		Go-Go	23.07 ± 2.09	15.4%	0.006*	1.73	Very Large
		LO	21.22 ± 2.07	8.0%	0.145	0.83	Large
		EEBA	19.53 ± 2.01				
	0.03 m	RC	54.03 ± 11.28	60.4%	< .001*	4.03	Huge
		Go-Go	27.13 ± 1.53	21.1%	< .001*	3.34	Huge
		LO	24.98 ± 2.38	14.3%	0.008*	1.66	Very Large
		EEBA	21.41 ± 1.88				
	0.02 m	RC	54.87 ± 8.54	56.4%	< .001*	4.71	Huge
		Go-Go	–	–	–	–	–
		LO	27.67 ± 3.59	13.6%	0.07	1.04	Large
		EEBA	23.90 ± 3.67				

Table B.8
t_2 results for each condition. Asterisks denote statistical significance.

D_m	Precision	Method	Avg. ± std.	$(M_i - M_{EEBA})/M_i$	p	Cohen's d	Effect size
2 m	0.05 m	RC	7.37 ± 0.91	55.5%	< .001*	5.31	Huge
		Go-Go	5.16 ± 0.52	36.5%	< .001*	3.36	Huge
		LO	3.38 ± 0.68	3.1%	0.77	0.16	Very Small
		EEBA	3.28 ± 0.60				
	0.03 m	RC	8.42 ± 1.20	36.1%	< .001*	2.25	Huge
		Go-Go	7.92 ± 1.20	32.1%	0.003*	1.88	Very Large
		LO	6.77 ± 1.06	20.1%	0.06	1.07	Large
		EEBA	5.38 ± 1.49				
	0.02 m	RC	9.25 ± 0.98	29.8%	< .001*	2.77	Huge
		Go-Go	9.42 ± 1.17	31.1%	< .001*	2.68	Huge
		LO	8.56 ± 1.05	24.1%	0.002*	2.01	Huge
		EEBA	6.50 ± 1.01				

(continued on next page)

Table B.8 (*continued*).

D_m	Precision	Method	Avg. ± std.	$(M_i - M_{EEBA})/M_i$	p	Cohen's d	Effect size
6 m	0.05 m	RC	5.24 ± 1.28	20.4%	0.35	0.51	Medium
		Go-Go	22.00 ± 10.87	81.0%	< .001*	2.25	Huge
		LO	15.88 ± 3.23	73.7%	< .001*	3.96	Huge
		EEBA	4.17 ± 2.66				
	0.03 m	RC	11.05 ± 2.60	31.2%	0.15	0.82	Large
		Go-Go	32.34 ± 16.65	76.5%	0.002*	2.00	Very Large
		LO	19.74 ± 6.38	61.5%	0.002*	2.06	Huge
		EEBA	7.61 ± 5.35				
	0.02 m	RC	19.92 ± 3.40	38.4%	0.03*	1.28	Very Large
		Go-Go	64.05 ± 21.42	80.8%	< .001*	3.21	Huge
		LO	41.15 ± 8.39	70.2%	< .001*	3.57	Huge
		EEBA	12.27 ± 7.76				
10 m	0.05 m	RC	21.20 ± 1.06	42.1%	< .001*	6.06	Huge
		Go-Go	30.28 ± 2.78	59.5%	< .001*	7.70	Huge
		LO	22.00 ± 0.88	44.2%	< .001*	6.88	Huge
		EEBA	12.27 ± 1.79				
	0.03 m	RC	33.95 ± 6.84	38.8%	< .001*	2.34	Huge
		Go-Go	64.45 ± 7.27	67.8%	< .001*	7.42	Huge
		LO	38.33 ± 4.15	45.8%	< .001*	4.28	Huge
		EEBA	20.77 ± 4.05				
	0.02 m	RC	53.33 ± 2.98	49.9%	< .001*	8.15	Huge
		Go-Go	–	–	–	–	–
		LO	43.94 ± 10.07	39.2%	< .001*	2.28	Huge
		EEBA	26.72 ± 3.53				

Table B.9
Approach Path Length results for each condition. Asterisks denote statistical significance.

D_m	Precision	Method	Avg. ± std.	$(M_i - M_{EEBA})/M_i$	p	Cohen's d	Effect size
2 m	0.05 m	RC	25.88 ± 3.23	68.1%	< .001*	5.49	Huge
		Go-Go	15.73 ± 2.77	47.5%	< .001*	2.50	Huge
		LO	8.28 ± 1.64	0.2%	0.99	0.007	Very Small
		EEBA	8.26 ± 3.19				
	0.03 m	RC	25.87 ± 2.96	68.5%	< .001*	5.91	Huge
		Go-Go	14.92 ± 2.85	45.4%	< .001*	2.30	Huge
		LO	9.58 ± 2.73	15.0%	0.37	0.50	Small
		EEBA	8.14 ± 3.04				
	0.02 m	RC	30.30 ± 4.69	71.6%	< .001*	6.03	Huge
		Go-Go	17.40 ± 3.22	50.5%	< .001*	3.30	Huge
		LO	12.83 ± 4.11	32.9%	0.028*	1.31	Very Large
		EEBA	8.61 ± 1.96				
6 m	0.05 m	RC	46.98 ± 4.62	60.9%	< .001*	8.28	Huge
		Go-Go	25.07 ± 3.28	26.8%	< .001*	2.60	Huge
		LO	22.38 ± 1.13	17.9%	< .001*	2.92	Huge
		EEBA	18.37 ± 1.58				
	0.03 m	RC	46.98 ± 9.80	61.6%	< .001*	4.17	Huge
		Go-Go	24.57 ± 2.07	26.6%	< .001*	4.25	Huge
		LO	21.4 ± 1.88	15.8%	< .001*	2.39	Huge
		EEBA	18.03 ± 0.67				
	0.02 m	RC	44.45 ± 9.29	60.4%	< .001*	4.06	Huge
		Go-Go	24.74 ± 1.68	28.8%	< .001*	5.06	Huge
		LO	24.12 ± 1.42	26.9%	< .001*	5.17	Huge
		EEBA	17.63 ± 1.07				
10 m	0.05 m	RC	86.98 ± 9.80	55.8%	< .001*	6.33	Huge
		Go-Go	64.45 ± 7.27	40.4%	< .001*	4.26	Huge
		LO	50.87 ± 5.76	24.5%	< .001*	2.38	Huge
		EEBA	38.42 ± 4.66				
	0.03 m	RC	98.33 ± 8.77	56.7%	< .001*	6.37	Huge
		Go-Go	80.99 ± 10.67	47.4%	< .001*	3.94	Huge
		LO	62.09 ± 10.21	31.4%	0.002*	2.05	Huge
		EEBA	42.58 ± 8.74				
	0.02 m	RC	102.69 ± 9.80	46.5%	< .001*	5.80	Huge
		Go-Go	–	–	–	–	–
		LO	67.05 ± 8.68	18.1%	0.010*	1.60	Very Large
		EEBA	54.90 ± 6.29				

Table B.10
Fine-tuning Path Length (m) results for each condition. Asterisks denote statistical significance.

D_m	Precision	Method	Avg. ± std.	$(M_i - M_{EEBA})/M_i$	p	Cohen's d	Effect size
2 m	0.05m	RC	3.23 ± 0.56	76.8%	< .001*	5.46	Huge
		Go-Go	2.86 ± 1.08	73.9%	< .001*	2.65	Huge
		LO	1.75 ± 0.53	57.2%	< .001*	2.27	Huge
		EEBA	0.75 ± 0.32				
	0.03 m	RC	4.42 ± 2.75	76.6%	0.005*	1.73	Very Large
		Go-Go	4.02 ± 1.95	74.3%	0.001*	2.14	Huge
		LO	3.00 ± 1.21	65.6%	0.001*	2.22	Huge
		EEBA	1.03 ± 0.30				
	0.02 m	RC	6.27 ± 2.37	43.7%	0.013*	1.51	Very Large
		Go-Go	8.77 ± 1.35	59.8%	< .001*	4.47	Huge
		LO	5.81 ± 1.36	39.2%	0.003*	1.93	Very Large
		EEBA	3.53 ± 0.96				
6 m	0.05 m	RC	4.32 ± 2.72	81.2%	0.005*	1.80	Very Large
		Go-Go	6.84 ± 6.12	88.2%	0.021*	1.39	Very Large
		LO	4.84 ± 3.55	83.2%	0.010*	1.59	Very Large
		EEBA	18.37 ± 1.58				
	0.03 m	RC	8.17 ± 5.08	85.7%	0.003*	1.94	Very Large
		Go-Go	7.09 ± 3.78	83.5%	0.001*	2.20	Huge
		LO	5.40 ± 2.34	78.3%	< .001*	2.51	Huge
		EEBA	1.17 ± 0.45				
	0.02 m	RC	8.85 ± 4.41	46.7%	0.037*	1.23	Very Large
		Go-Go	13.27 ± 3.99	64.5%	< .001*	2.78	Huge
		LO	7.15 ± 1.93	34.0%	0.027*	1.32	Very Large
		EEBA	4.72 ± 1.73				
10 m	0.05 m	RC	9.07 ± 3.71	50.5%	0.011*	1.57	Very Large
		Go-Go	11.21 ± 7.01	60.0%	0.028*	1.31	Very Large
		LO	8.59 ± 3.45	47.8%	0.015*	1.49	Very Large
		EEBA	4.49 ± 1.83				
	0.03 m	RC	8.46 ± 4.54	48.1%	0.038*	1.23	Very Large
		Go-Go	13.84 ± 4.99	68.3%	< .001*	2.61	Huge
		LO	9.52 ± 4.06	53.9%	0.006*	1.72	Very Large
		EEBA	4.39 ± 1.18				
	0.02 m	RC	13.02 ± 3.33	49.2%	< .001*	2.23	Huge
		Go-Go	–	–	–	–	–
		LO	10.78 ± 2.49	38.6%	0.006*	1.73	Very Large
		EEBA	6.62 ± 2.33				

References

Abtahi, P., Gonzalez-Franco, M., Ofek, E., Steed, A., 2019. I'm a giant: Walking in large virtual environments at high speed gains. In: Proceedings of the 2019 CHI Conference on Human Factors in Computing Systems. CHI '19, Association for Computing Machinery, New York, NY, USA, pp. 1–13. http://dx.doi.org/10.1145/3290605.3300752.

Bolte, B., Steinicke, F., Bruder, G., 2011. The jumper metaphor: An effective navigation technique for immersive display setups. In: Proceedings of Virtual Reality International Conference.

Bowman, D.A., Hodges, L.F., 1997. An evaluation of techniques for grabbing and manipulating remote objects in immersive virtual environments. In: Proceedings of the 1997 Symposium on Interactive 3D Graphics. pp. 35–ff.

Bowman, D.A., Johnson, D.B., Hodges, L.F., 1999. Testbed evaluation of virtual environment interaction techniques. In: Proceedings of the ACM Symposium on Virtual Reality Software and Technology. VRST '99, Association for Computing Machinery, New York, NY, USA, pp. 26–33. http://dx.doi.org/10.1145/323663.323667.

Bozgeyikli, E., Raij, A., Katkoori, S., Dubey, R., 2016. Point & teleport locomotion technique for virtual reality. In: Proceedings of the 2016 Annual Symposium on Computer-Human Interaction in Play. pp. 205–216.

Chatterjee, I., Xiao, R., Harrison, C., 2015. Gaze+ gesture: Expressive, precise and targeted free-space interactions. In: Proceedings of the 2015 ACM on International Conference on Multimodal Interaction. pp. 131–138.

Cohen, J., 2013. Statistical Power Analysis for the Behavioral Sciences. Routledge.

Dewez, D., Hoyet, L., Lécuyer, A., Argelaguet, F., 2022. Do you need another hand? Investigating dual body representations during anisomorphic 3D manipulation. IEEE Trans. Vis. Comput. Graphics 28 (5), 2047–2057. http://dx.doi.org/10.1109/TVCG.2022.3150501.

Feuchtner, T., Müller, J., 2017. Extending the body for interaction with reality. In: Proceedings of the 2017 CHI Conference on Human Factors in Computing Systems. pp. 5145–5157.

Feuchtner, T., Müller, J., 2018. Ownershift: Facilitating overhead interaction in virtual reality with an ownership-preserving hand space shift. In: Proceedings of the 31st Annual ACM Symposium on User Interface Software and Technology. pp. 31–43.

Franklin, D.W., Wolpert, D.M., 2011. Computational mechanisms of sensorimotor control. Neuron 72 (3), 425–442.

Frees, S., Kessler, G.D., 2005. Precise and rapid interaction through scaled manipulation in immersive virtual environments. In: IEEE Proceedings. VR 2005. Virtual Reality, 2005. IEEE, pp. 99–106.

Graham, E.D., MacKenzie, C.L., 1996. Physical versus virtual pointing. In: Proceedings of the SIGCHI Conference on Human Factors in Computing Systems. pp. 292–299.

Hart, S., 2006. Nasa-task load index (NASA-TLX); 20 years later. In: Proceedings of the Human Factors and Ergonomics Society Annual Meeting, vol. 50, pp. 904–908.

Hart, S., Staveland, L., 1988. Development of NASA-TLX (Task Load Index): Results of empirical and theoretical research. Adv. Psychol. 52, 139–183.

Hincapié-Ramos, J.D., Guo, X., Moghadasian, P., Irani, P., 2014. Consumed endurance: A metric to quantify arm fatigue of mid-air interactions. In: Proceedings of the SIGCHI Conference on Human Factors in Computing Systems. pp. 1063–1072.

Jacoby, R.H., Ferneau, M., Humphries, J., 1994. Gestural interaction in a virtual environment. In: Stereoscopic Displays and Virtual Reality Systems, vol. 2177, SPIE, pp. 355–364.

Jiang, F., Yang, X., Feng, L., 2016. Real-time full-body motion reconstruction and recognition for off-the-shelf VR devices. In: Proceedings of the 15th ACM SIGGRAPH Conference on Virtual-Reality Continuum and Its Applications in Industry-Volume 1. pp. 309–318.

Kim, H., Lee, G.A., Billinghurst, M., 2015. A non-linear mapping technique for bare-hand interaction in large virtual environments. In: Australasian Computer-Human Interaction Conference.

Li, J., Cho, I., Wartell, Z., 2015. Evaluation of 3d virtual cursor offset techniques for navigation tasks in a multi-display virtual environment. In: 2015 IEEE Symposium on 3D User Interfaces. 3DUI, IEEE, pp. 59–66.

Li, J., Cho, I., Wartell, Z., 2018. Evaluation of cursor offset on 3D selection in VR. In: Proceedings of the Symposium on Spatial User Interaction. pp. 120–129.

Li, N., Zhang, Z., Liu, C., Yang, Z., Fu, Y., Tian, F., Han, T., Fan, M., 2021. Vmirror: Enhancing the interaction with occluded or distant objects in VR with virtual mirrors. In: Proceedings of the 2021 CHI Conference on Human Factors in Computing Systems. pp. 1–11.

Liu, X., Wang, L., Luan, S., Shi, X., Liu, X., 2022. Distant object manipulation with adaptive gains in virtual reality. In: 2022 IEEE International Symposium on Mixed and Augmented Reality. ISMAR, IEEE, pp. 739–747.

McAtamney, L., Corlett, E.N., 1993. RULA: A survey method for the investigation of work-related upper limb disorders. Appl. Ergonomics 24 (2), 91–99.

Mendes, D., Caputo, F.M., Giachetti, A., Ferreira, A., Jorge, J., 2019. A survey on 3d virtual object manipulation: From the desktop to immersive virtual environments. In: Computer Graphics Forum. Wiley Online Library, pp. 21–45.

Mine, M.R., 1995. Virtual Environment Interaction Techniques. UNC Chapel Hill CS Dept, Citeseer.

Montano Murillo, R.A., Subramanian, S., Martinez Plasencia, D., 2017. Erg-O: Ergonomic optimization of immersive virtual environments. In: Proceedings of the 30th Annual ACM Symposium on User Interface Software and Technology. pp. 759–771.

Morrey, B.F., An, K., Chao, E., 2000. Functional evaluation of the elbow. In: Morrey, B.F., Sanchez-351 Sotelo, J., Morrey, M.E. (Eds.), In: Morrey's the Elbow and its Disorders, vol. 352, pp. 66–74.

Morrey, B., Askew, L., Chao, E., 1981. A biomechanical study of normal functional elbow motion. J. Bone Joint Surg.. Am. Vol. 63 (6), 872–877.

Parger, M., Mueller, J.H., Schmalstieg, D., Steinberger, M., 2018. Human upper-body inverse kinematics for increased embodiment in consumer-grade virtual reality. In: Proceedings of the 24th ACM Symposium on Virtual Reality Software and Technology. pp. 1–10.

Pierce, J.S., Forsberg, A.S., Conway, M.J., Hong, S., Zeleznik, R.C., Mine, M.R., 1997. Image plane interaction techniques in 3D immersive environments. In: Proceedings of the 1997 Symposium on Interactive 3D Graphics. pp. 39–ff.

Pierce, J.S., Stearns, B.C., Pausch, R., 1999. Voodoo dolls: Seamless interaction at multiple scales in virtual environments. In: Proceedings of the 1999 Symposium on Interactive 3D Graphics. pp. 141–145.

Pohl, H., Lilija, K., McIntosh, J., Hornbæk, K., 2021. Poros: Configurable proxies for distant interactions in VR. In: Proceedings of the 2021 CHI Conference on Human Factors in Computing Systems. CHI '21, Association for Computing Machinery, New York, NY, USA, http://dx.doi.org/10.1145/3411764.3445685.

Poupyrev, I., Billinghurst, M., Weghorst, S., Ichikawa, T., 1996. The go-go interaction technique: Non-linear mapping for direct manipulation in VR. In: Proceedings of the 9th Annual ACM Symposium on User Interface Software and Technology. pp. 79–80.

Rosenbaum, D.A., 2009. Human Motor Control. Academic Press.

Schmidt, R.A., Wrisberg, C.A., 2008. Motor Learning and Performance: A Situation-Based Learning Approach. Human kinetics.

Spanlang, B., Normand, J.M., Giannopoulos, E., Slater, M., 2010. A first person avatar system with haptic feedback. In: Proceedings of the 17th ACM Symposium on Virtual Reality Software and Technology. pp. 47–50.

Stoakley, R., Conway, M.J., Pausch, R., 1995. Virtual reality on a WIM: Interactive worlds in miniature. In: Proceedings of the SIGCHI Conference on Human Factors in Computing Systems. pp. 265–272.

Sun, J., Stuerzlinger, W., 2019. Extended sliding in virtual reality. In: Proceedings of the 25th ACM Symposium on Virtual Reality Software and Technology. VRST '19, Association for Computing Machinery, New York, NY, USA, http://dx.doi.org/10.1145/3359996.3364251.

Sun, J., Stuerzlinger, W., Shuralyov, D., 2016. SHIFT-sliding and DEPTH-POP for 3D positioning. In: Proceedings of the 2016 Symposium on Spatial User Interaction. SUI '16, Association for Computing Machinery, New York, NY, USA, pp. 69–78. http://dx.doi.org/10.1145/2983310.2985748.

Turner, J., Alexander, J., Bulling, A., Schmidt, D., Gellersen, H., 2013. Eye pull, eye push: Moving objects between large screens and personal devices with gaze and touch. In: Human-Computer Interaction–INTERACT 2013: 14th IFIP TC 13 International Conference, Cape Town, South Africa, September 2-6, 2013, Proceedings, Part II 14. Springer, pp. 170–186.

Turner, J., Bulling, A., Gellersen, H., 2011. Combining gaze with manual interaction to extend physical reach. In: Proceedings of the 1st International Workshop on Pervasive Eye Tracking & Mobile Eye-Based Interaction. pp. 33–36.

Velloso, E., Turner, J., Alexander, J., Bulling, A., Gellersen, H., 2015. An empirical investigation of gaze selection in mid-air gestural 3D manipulation. In: Human-Computer Interaction–INTERACT 2015: 15th IFIP TC 13 International Conference, Bamberg, Germany, September 14-18, 2015, Proceedings, Part II 15. Springer, pp. 315–330.

Voelker, S., Hueber, S., Holz, C., Remy, C., Marquardt, N., 2020. GazeConduits: Calibration-free cross-device collaboration through gaze and touch. In: Proceedings of the 2020 CHI Conference on Human Factors in Computing Systems. pp. 1–10.

Wentzel, J., d'Eon, G., Vogel, D., 2020. Improving virtual reality ergonomics through reach-bounded non-linear input amplification. In: Proceedings of the 2020 CHI Conference on Human Factors in Computing Systems. pp. 1–12.

Wilkes, C., Bowman, D.A., 2008. Advantages of velocity-based scaling for distant 3D manipulation. In: Proceedings of the 2008 ACM Symposium on Virtual Reality Software and Technology. VRST '08, Association for Computing Machinery, New York, NY, USA, pp. 23–29. http://dx.doi.org/10.1145/1450579.1450585.

Winkler, A., Won, J., Ye, Y., 2022. QuestSim: Human motion tracking from sparse sensors with simulated avatars. In: SIGGRAPH Asia 2022 Conference Papers. pp. 1–8.

Yi, X., Zhou, Y., Habermann, M., Shimada, S., Golyanik, V., Theobalt, C., Xu, F., 2022. Physical inertial poser (pip): Physics-aware real-time human motion tracking from sparse inertial sensors. In: Proceedings of the IEEE/CVF Conference on Computer Vision and Pattern Recognition. pp. 13167–13178.

Yu, R., Bowman, D.A., 2018. Force push: Exploring expressive gesture-to-force mappings for remote object manipulation in virtual reality. Front. ICT 5, 25.

Yu, D., Liang, H.N., Fan, K., Zhang, H., Fleming, C., Papangelis, K., 2019. Design and evaluation of visualization techniques of off-screen and occluded targets in virtual reality environments. IEEE Trans. Vis. Comput. Graph. 26 (9), 2762–2774.

Yu, D., Lu, X., Shi, R., Liang, H.-N., Dingler, T., Velloso, E., Goncalves, J., 2021. Gaze-supported 3d object manipulation in virtual reality. In: Proceedings of the 2021 CHI Conference on Human Factors in Computing Systems. pp. 1–13.

Yu, D., Zhou, Q., Newn, J., Dingler, T., Velloso, E., Goncalves, J., 2020. Fully-occluded target selection in virtual reality. IEEE Trans. Vis. Comput. Graph. 26 (12), 3402–3413.